Multimerization of PyCSP for Novel Malaria Vaccine Antigens

Suzannah Beeman

A thesis

submitted in partial fulfillment of the

requirements for the degree of

Master of Science

University of Washington

2023

Committee:

Noah Sather

Daniel Ratner

Program Authorized to Offer Degree:

Bioengineering

University of Washington

ABSTRACT

Multimerization of PyCSP for Novel Malaria Vaccine Antigens

Suzannah Beeman

Chair of the Supervisory Committee:
Noah Sather
Departments of Pediatrics and Global Health

Current experimental vaccines against malaria have demonstrated a limited capacity to elicit a durable protective immune response capable of diminishing infection and transmission in endemic regions. The use of virus-like particles to produce multimerized vaccine antigens is a promising approach for improving the quality and durability of vaccine-elicited immune responses against several pathogens, including in experimental vaccines for malaria. The Sather lab has studied various malaria antigens and their interactions with various antibodies, with a goal of identifying a vaccine target that will elicit antibodies capable of providing patients with protective immunity against malaria. This study will focus on constructing and testing the immunogenicity and efficacy of multimerization strategies of the circumsporozoite (CSP) protein against a recombinant CSP monomeric antigen. Antigen constructs encoding for antigens of increasing valency were designed and evaluated *in vitro* and *in vivo* and anti-vaccine serum antibody responses were assessed for antibody binding titers, binding avidity, and antibody subclass distribution.

I. INTRODUCTION

Malaria is a deadly disease with a devastating impact in many parts of the world, primarily in tropical regions such as Africa, South America, and South Asia. There are 84 countries in malaria risk zones as identified by the 2022 WHO World Malaria Report, which includes nearly half of the world's population [1]. Sub-Saharan Africa represents the highest occurrence of deaths and infections of malaria, with pregnant women and children being the most vulnerable. In 2021, there were 247 million people hospitalized and 619,000 dead of malaria, 95% of which were in Africa [1]. Malaria also has a devastating economic impact in the many countries it affects. People afflicted by the disease must purchase drugs for treatment, travel to clinics for treatment, and take time away from work, which can be costly. Additionally, governments must take on the costs of health facilities and supplies, public health initiatives, infrastructure, and lost business and tourism opportunities. The CDC has estimated the direct costs of malaria to be at least $12 billion USD worldwide per year, which does not account for the substantial cost of lost economic growth caused by malaria [2].

Malaria is a difficult disease to target through vaccines due to its complex life cycle. The infection is caused by Plasmodium parasites, which are injected into the body by a bite from a female Anopheles mosquito during a blood meal. After injection, the parasite is in its sporozoite form, and invades the vasculature and transits to the liver, where it infects hepatocytes and replicates the blood stage schizont form. After this phase, the parasites leave the liver in the form of merozoites, where the blood phase begins as red blood cells are infected, causing the illness symptoms commonly associated with malaria disease. The parasites in infected cells then can develop into gametocytes, which are ingested by mosquitos and the cycle repeats [3]. Because

there are so many stages of the parasite's life cycle, there are many potential vaccine targets. One area of focus is on the asymptomatic pre-erythrocytic sporozoite phase, with a goal of targeting the malaria infection before it reaches the liver, which would prevent infection and break the transmission cycle. This makes the circumsporozoite protein (CSP), found in abundance on the surface of the sporozoite, an ideal target for vaccines.

The most notable recent development in the field of malaria vaccine research is the approval of the RTS,S malaria vaccine by the World Health Organization as of October 2021. The vaccine targets the parasite *Plasmodium falciparum*, which causes the deadliest form of malaria. It has been determined to be feasible, cost-effective, and safe for children [4]. However, there is still work to be done in this field, as it currently only achieves partial protection from clinical disease and little protection from infection. The RTS,S vaccine is composed of a virus-like particle constructed by assembling parts of CSP from *P. falciparum* to the scaffold Hepatitis B surface antigen and combined with AS01 adjuvant. Vaccination with RTS,S occurs in four doses and has a protection rate against clinical disease of 36% for infants across four years [5]. In the present study, the goal is to test a variety of different multimerization schemes—including higher order multimerizations—to increase vaccine efficacy.

In previous studies, fusing protein to the oligomerization domain for the heptameric C4-binding protein (C4bp), an abundant plasma protein that naturally functions to inhibit the classical and lectin pathways of complement activation, has resulted in enhanced protective immunity in BALB/c mice when compared to purified protein antigens [6]. The fusion of C4bp's oligomerization domain to malaria antigens has also been shown to induce more T cell activity,

albeit with no improvement of functional antibody response [7]. These prior observations provide a strong rationale to investigate the effects of conjugating CSP—a malaria antigen of interest—to C4bp, as well as higher-order multimers. In addition to C4bp, the exploration of oligomerized and multimerized proteins is well-characterized in the literature, with many effective methods of production and evaluation of these constructs [8].

As a result, the overarching aim of this project is the use of self-assembling protein structures to multimerize vaccine antigens. These constructs are promising for next-generation vaccines, as they are highly versatile and have been shown to enhance immunity and stimulation of B cells. Their structures can allow them to mimic a variety of pathogens without incurring the same risk as a real pathogen. They are also ideal for stability and repetitive antigen display, important factors to consider for the development of multimerization schemes [9]. Additionally, larger particles enable antigens to be efficiently captured, transported to B cells, potentially resulting in enhanced maturation of B cells [9]. As a result, larger antigens have the potential to elicit a more robust and durable antibody response. Such protein structures have already shown promising results as multimerization platforms. A tag-and-display SpyCatcher-mi3 fusion scaffold was developed using the previously-characterized SpyCatcher-SpyTag isopeptide bonding system and mi3, a mutated version of the i301 porous dodecahedral 60-mer [10]. This construct proved highly stable in many conditions, including freezing, thawing, lyophilization, and long-term storage. It also demonstrated a 95% coupling efficiency with malaria antigens. There was also high binding avidity and antibody response when this protein scaffold was conjugated with the *P. falciparum* CyRPA protein [10].

Given this information, this study will focus on designing and constructing multimerized forms of CSP in varying degrees of antigen multiplicity and testing their vaccine efficacy against monomeric CSP. For the purpose of this study, efficacy will be evaluated using mouse models, and therefore the specific antigen of interest is *Plasmodium yoelii* CSP (PyCSP), the circumsporozoite protein from a mouse strain of malaria.

II. WHOLE PYCSP MULTIMERIZATION

In this study, the effects of multimerization on the immunogenic properties of PyCSP were investigated. Various degrees of multimerization were investigated by genetically fusing PyCSP to other proteins. A heptamer was constructed using C4bp, a 24mer using ferritin, and 60mers using lumazine synthase and SpyCatcher-mi3. The variant of C4bp used was IMX313, a heptamer comprising a hybridized oligomerization domain of chicken C4bp and human C4bp, with 21% homology to the human protein [11]. The ferritin construct was modified from a previously characterized PvCSP-ferritin fusion plasmid in a pcDNA3.4 vector by restriction digest and Gibson assembly. The lumazine synthase construct was generated through genetic fusion of the sequence of lumazine synthase derived from *Aquifex aeolicus* (AaLS) into a pcDNA3.4 backbone expressing PyCSP. All of these are self-assembling virus-like particles, with the exception of the SpyCatcher-mi3 construct; however, this construct was unsuccessful in PyCSP conjugation and therefore was ultimately not pursued. Additionally, the ferritin and lumazine synthase constructs failed to form PyCSP-expressing nanoparticles using genetic fusion.

A general diagram for self-assembling nanoparticle generation is shown in Figure 1. Each subunit is conjugated to a copy of the target antigen, resulting in a nanoparticle expressing multiple copies of the antigen after its subunits assemble. Ideally, this process happens spontaneously and particles remain intact under physiological conditions. The number of antigen copies expressed will depend on the scaffold. For example, ferritin has 24 subunits and could potentially express 24 copies while lumazine synthase has 60 subunits and could potentially express 60 copies. However, especially for larger protein antigens such as PyCSP, it is unlikely that all subunits will express an antigen after assembly.

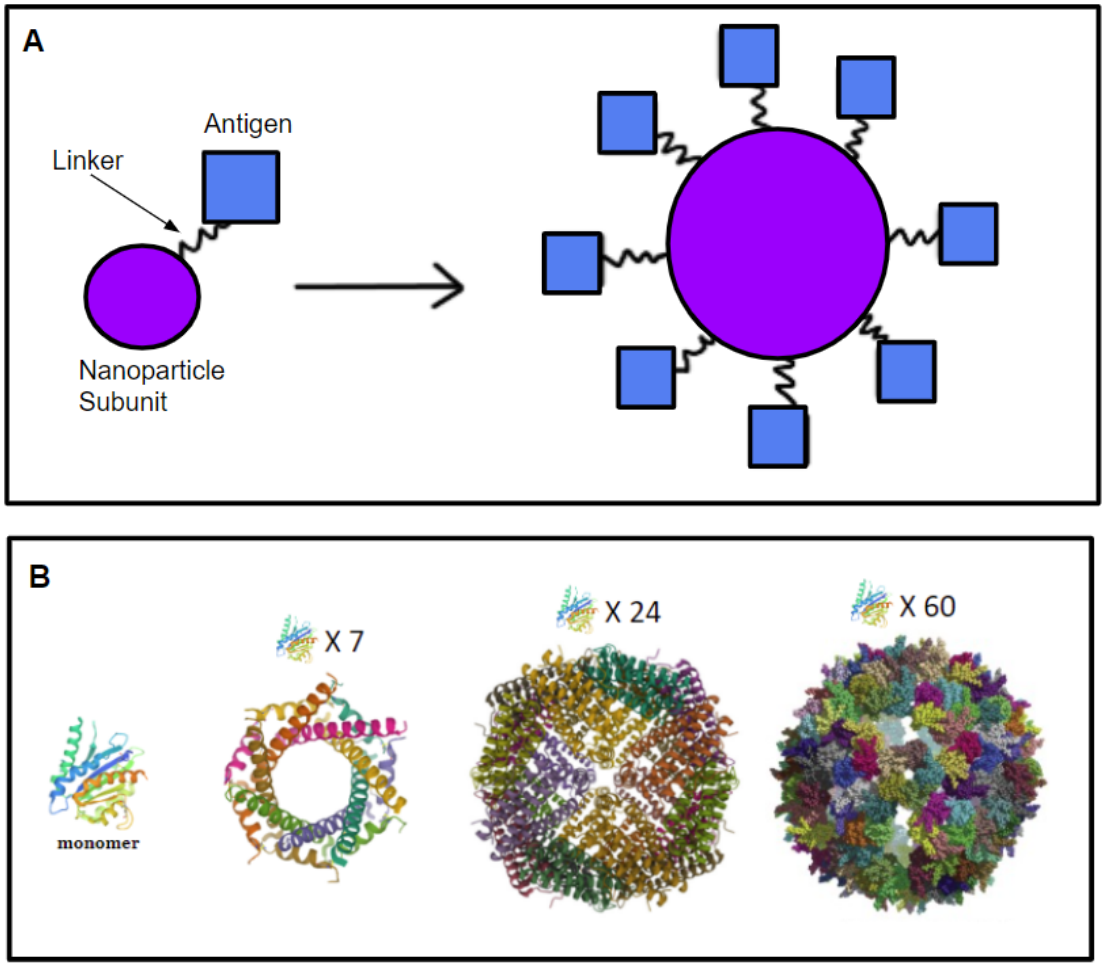

Figure 1: Panel A is a diagram showing self-assembly of nanoparticles. Each individual subunit is conjugated to a target antigen by a linker sequence, resulting in a large particle expressing multiple copies of an antigen after assembly. The number of antigen copies expressed will depend on the scaffold. For example, ferritin has 24 subunits and could potentially express 24 copies while lumazine synthase has 60 subunits and could potentially express 60

copies. However, especially for larger protein antigens such as PyCSP, it is unlikely that all subunits will express an antigen after assembly. Panel B is a schematic representing the various nanoparticle sizes referenced in this study.

Results and Discussion

With the exception of the C-terminally conjugated lumazine synthase construct, all plasmids were successfully constructed and verified through Nco1 digest and Sanger sequencing. Some constructs required multiple cloning attempts, but by optimizing vector:insert ratios and *E. coli* transformation protocol, plasmid modification and expression was accomplished.

An example of an Nco1 digest verification is shown in Figure 2 with the lumazine synthase constructs. When compared to the expected band sizes, one of the N terminally fused clones (AaLS-PyCSP) displays the characteristic band at 2000 base pairs, while the other clone and both C terminally fused clones (PyCSP-AaLS) do not display this band and instead bear closer resemblance to the parent PyCSP plasmid with characteristic band at approximately 1500 base pairs. This indicates that the first N terminally fused clone is a successfully constructed plasmid while the others are not. This was later confirmed through Sanger DNA sequencing.

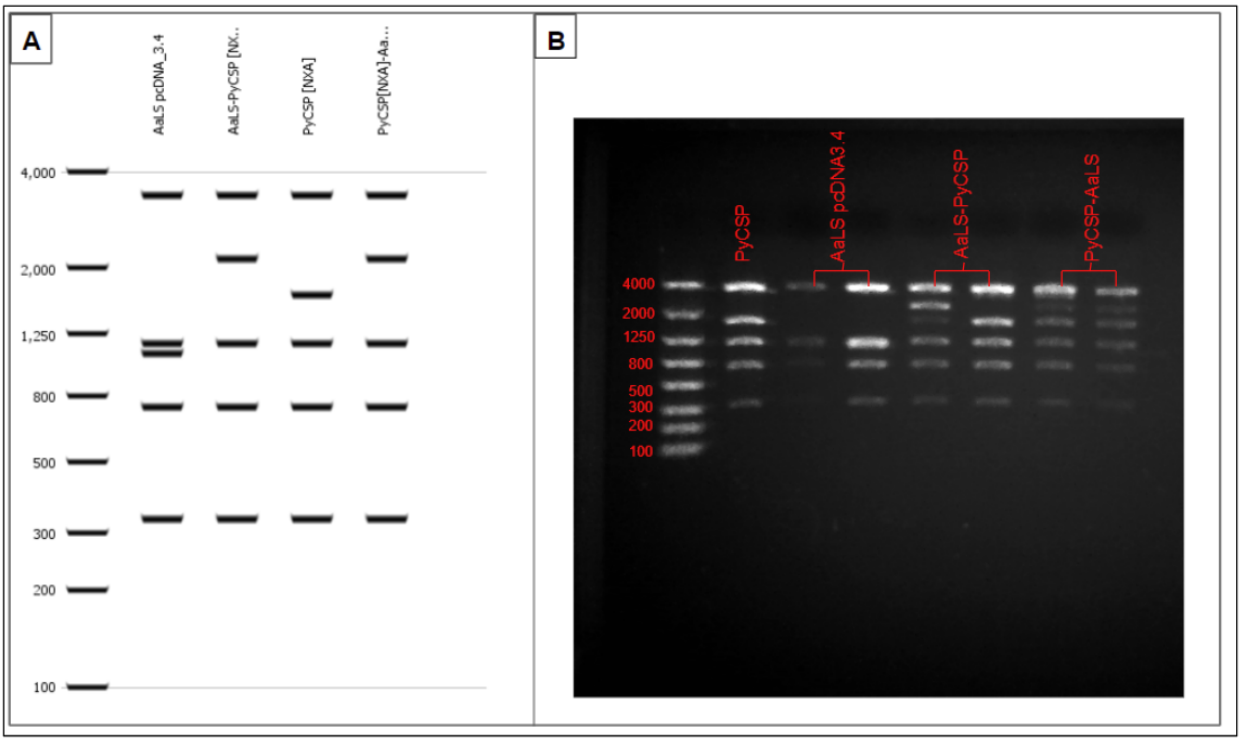

Figure 2: Panel A shows a prediction of band sizes resulting from an Nco1 digest as computed by Geneious. From left to right: unconjugated lumazine synthase, N terminally fused lumazine synthase, PyCSP control, C terminally fused lumazine synthase. Panel B shows an image taken using the Lonza FlashGel™ system. Lane 1 is a ladder showing weight in DNA base pairs, Lane 2 is a PyCSP control, Lanes 3-4 are unconjugated lumazine synthase, Lanes 5-6 are N terminally fused lumazine synthase, and Lanes 7-8 are C terminally fused lumazine synthase.

After protein expression in HEK 293F cells, purification by Ni-NTA affinity chromatography, and subsequent analysis as specified in the methods section, only the IMX313 heptamer was successfully produced and verified in the available time frame. Figure 3 shows an SDS PAGE performed on the IMX313 sample. The data was taken from various fractions of the IMX313 construct after size exclusion chromatography (SEC) was performed. As shown in fraction 9, the largest molecular weight out of the chosen samples, there is a distinction between the reducing condition showing the expected molecular weight for a single subunit, as well as higher molecular weight bands under non-reducing conditions. This indicates the presence of multimerization in this construct.

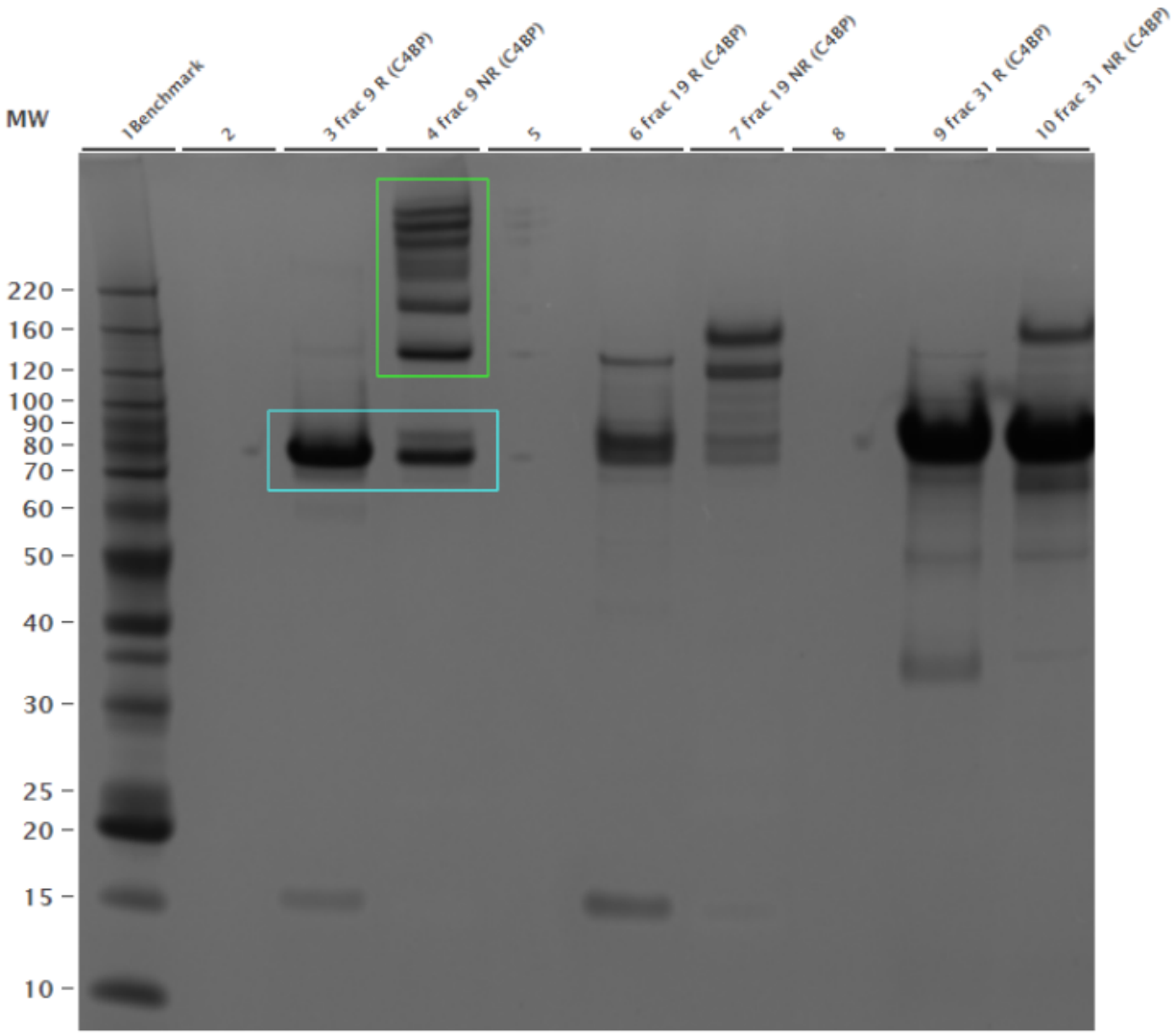

Figure 3: This SDS PAGE shows a comparison between reduced and non-reduced conditions at three different time points in an SEC run, with earlier fractions representing higher molecular weights. As highlighted in blue, Fraction 9 shows a band at about ~75 kDa under both reducing and non-reducing conditions. However, under non-reducing conditions, Fraction 9 shows other, higher molecular weight bands. This indicates the presence of a single subunit of PyCSP-IMX313 that assembles into a larger particle under non-reducing (physiological) conditions.

In attempting to purify the genetically fused ferritin construct, SDS PAGE analysis revealed that only material resembling PyCSP and no material resembling ferritin appeared in the sample after immobilized metal affinity chromatography (IMAC) was performed. This is potentially due to the cleavage of PyCSP at a site in the middle of the protein that has been characterized by previous work in the Sather lab. Because the histidine tag and ferritin were fused at opposite

ends of PyCSP, this cleavage would have caused the ferritin portion of the protein to be lost during the purification process.

The N-terminally fused construct of lumazine synthase failed to express in HEK 293F cells after multiple attempts at test expressions, and was abandoned early on in the project due to it being the most unfamiliar construct in the Sather lab and the uncertainty that a protein the size and shape of PyCSP would be able to successfully form into the anticipated 60mer.

For the SpyCatcher construct, both SpyCatcher003-mi3 and SpyTag003-PyCSP were verified to have expressed successfully through SEC and SDS PAGE. However, as demonstrated by Figure 4, when trying to conjugate the two components, the reaction was unsuccessful. Rather than assembling into a larger subunit, bands are observed at ~70 kDa and ~40 kDa, mirroring the controls for SpyTag003-PyCSP and SpyCatcher003-mi3 respectively.

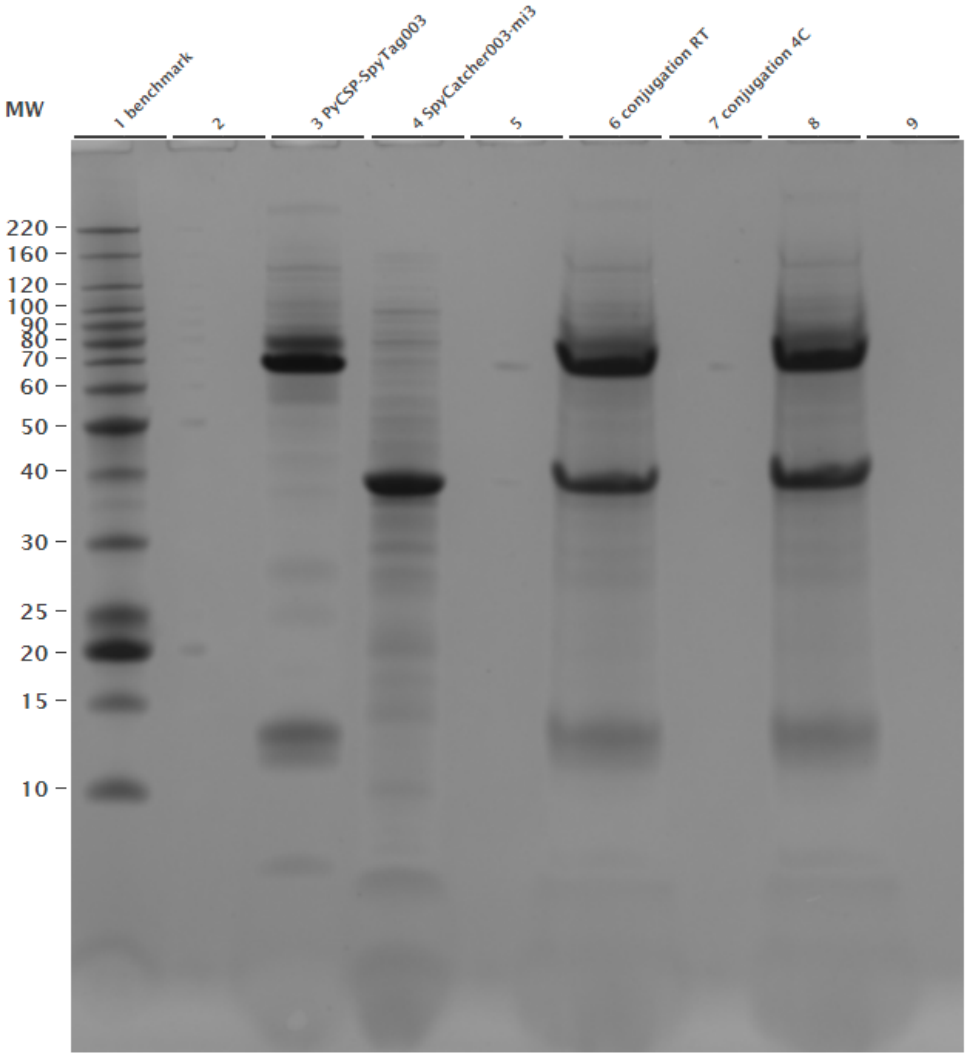

Figure 4: This SDS PAGE shows controls for the two components of the conjugation reaction (SpyTag003-PyCSP and SpyCatcher003-mi3 respectively) compared to two conjugation reactions: one performed at room temperature and the other at 4C. Both samples show the two components rather than a successfully assembled subunit.

Materials and Methods

i. Plasmid Design and Construction

Antigens were designed *in silico* using the Geneious software, which allowed the synthesis of known DNA sequences to generate models of novel proteins. The C terminus of PyCSP was joined to the oligomerization domain of C4bp, which has shown promise with other antigens [6]. A ferritin construct was generated by joining the N terminus of ferritin to the C terminus of PyCSP using a 10-residue GSG linker sequence as previously characterized with other antigens

[12]. An additional ferritin construct was used by fusing a peptide to the C terminus of PyCSP to act as a sortase A motif for later conjugation to ferritin through a reaction catalyzed by the sortase A enzyme; this method was selected due to its previous success with other antigens in the Sather lab. Two different constructs were designed for lumazine synthase; one fused to the N terminus of PyCSP using a 10-residue Ala-Ala linker sequence and the other fused to the C terminus of PyCSP using the linker sequence GGSGGSGGSGGSGGG. Both of these designs were based on previously characterized constructs in literature, and the fact that the surface exposure of both termini of lumazine synthase allows for conjugation at either end [13, 14]. The SpyCatcher003 construct was created from two separate components. The SpyCatcher003-mi3 plasmid (Addgene plasmid # 159995 ; http://n2t.net/addgene:159995 ; RRID:Addgene_159995) was a gift from Mark Howarth and required no additional modification [15]. The SpyTag003-mi3 plasmid was created by genetically fusing the SpyTag003 peptide to the C terminus of PyCSP. All plasmids were designed with an 8-residue histidine tag for later protein purification by IMAC.

Following plasmid design using Geneious, plasmids were constructed by performing restriction digests using NheI-HF (NEB #R3131S) and BamHI-HF (NEB #R3136S) enzymes on parent pcDNA3.4 plasmids, purifying DNA components using gel electrophoresis with a Lonza FlashGelTM system (cat. #57067). For the C4bp and ferritin constructs, all necessary components were available in the Sather lab. For the lumazine synthase and SpyTag003-PyCSP constructs, an existing PyCSP[NXA] plasmid was modified using synthetic DNA gBlocks that were first codon-optimized for mammalian expression in HEK 293F cells then ordered from Integrated DNA Technologies. Components were then mixed at a ratio of 1:2 vector:insert and

joined through Gibson assembly using HiFi Assembly Master Mix from New England Biolabs (cat. #E2621L). Then, plasmids were transformed into New England Biolabs 5-alpha C2987H cells and plated on antibiotic-treated agar plates. Colonies were then selected for extraction by miniprep using a NucleoSpin® plasmid purification kit (Macherey-Nagel #740588.250).

To verify successful construction of plasmids, Nco1 (NEB #R3193S) digests were performed and the digestion products were separated and analyzed by gel electrophoresis. The resulting band patterns were then compared to predicted DNA bands computed by Geneious. Promising constructs were then sent to Genewiz and Sanger sequencing was performed for additional verification. Sequences were aligned in Geneious and verified against our synthetic reference sequences.

ii. Protein Production and Purification

With the exception of SpyCatcher003-mi3, all verified plasmids were transfected into HEK 293F cells. For a 500mL cell culture in FreeStyle™ Expression Medium (Gibco #12338-018), 250uL of plasmid DNA was first left to incubate in a 20mL phosphate-buffered saline (PBS) solution with 666uL polyethylenimine MAX (MW = 40,000) for 15 minutes. Then, the solution was added to the cell culture (concentration of 1 million cells per mL) and left in a 37C shaking incubator for 3-4 days. The resulting supernatant was purified by IMAC using a Ni-NTA agarose column. Protein species were then separated by SEC using a Superdex 200 16/600 column. Finally, purified proteins were verified by SDS PAGE and Western blot analysis.

The SpyCatcher003-mi3 plasmid was transformed into E. coli cells and purified as previously described [15]. Following this process, protein purification was validated using SDS PAGE.

III. SORTASE A FERRITIN CONJUGATION

After the failure to generate ferritin nanoparticles using the genetically fused construct, a ferritin construct was designed to fuse PyCSP and ferritin using a sortase A (srtA) catalyzed transpeptidation reaction. VLPs are an emerging area of interest in the field of immunology, and previous studies show that they are more effective in eliciting neutralizing antibodies than monomeric protein antigens. Ferritin, often assembled through srtA reactions, specifically is noted as an effective platform due to its thermal stability. This reaction works by cleaving a C-terminal recognition tag (LPSTGG) between the two glycine residues and conjugating it to a complementary N-terminal penta-glycine tag [16, 17, 18]. SrtA also has the potential to be a highly versatile platform; any antigen expressing the complementary recognition tag can be conjugated to the same stock of ferritin. Furthermore, genetic fusion can result in complications such as improper protein folding and inability to effectively self-assemble [19]. Due to previous failures of genetic fusion in this project and the success of ferritin as an antigen platform when assembled through srtA reactions, this strategy showed promise in multimerizing PyCSP.

Results and Discussion

In this study, a ferritin construct with an N-terminal pentaglycine tag was conjugated with a PyCSP construct containing a LPSTGG tag at its C-terminus. A calcium-independent variant of the srtA enzyme was also used to allow for compatibility with HBS-E, a buffer that proteins are typically stored in. The reaction initially performed with poor conjugation efficiency. After

purification and the sortase A conjugation reaction were performed, the resulting sample was tested through SDS PAGE as shown in Figure 5. However, as seen in the figure, the SEC fractions representing the conjugated sample show two distinct bands as ~70 kDa and ~25 kDa highlighted in Figure 5), which are the expected values of molecular weight of PyCSP and ferritin respectively, as demonstrated by the controls. This suggests that no significant conjugation of the two components took place, and therefore no multimer formed.

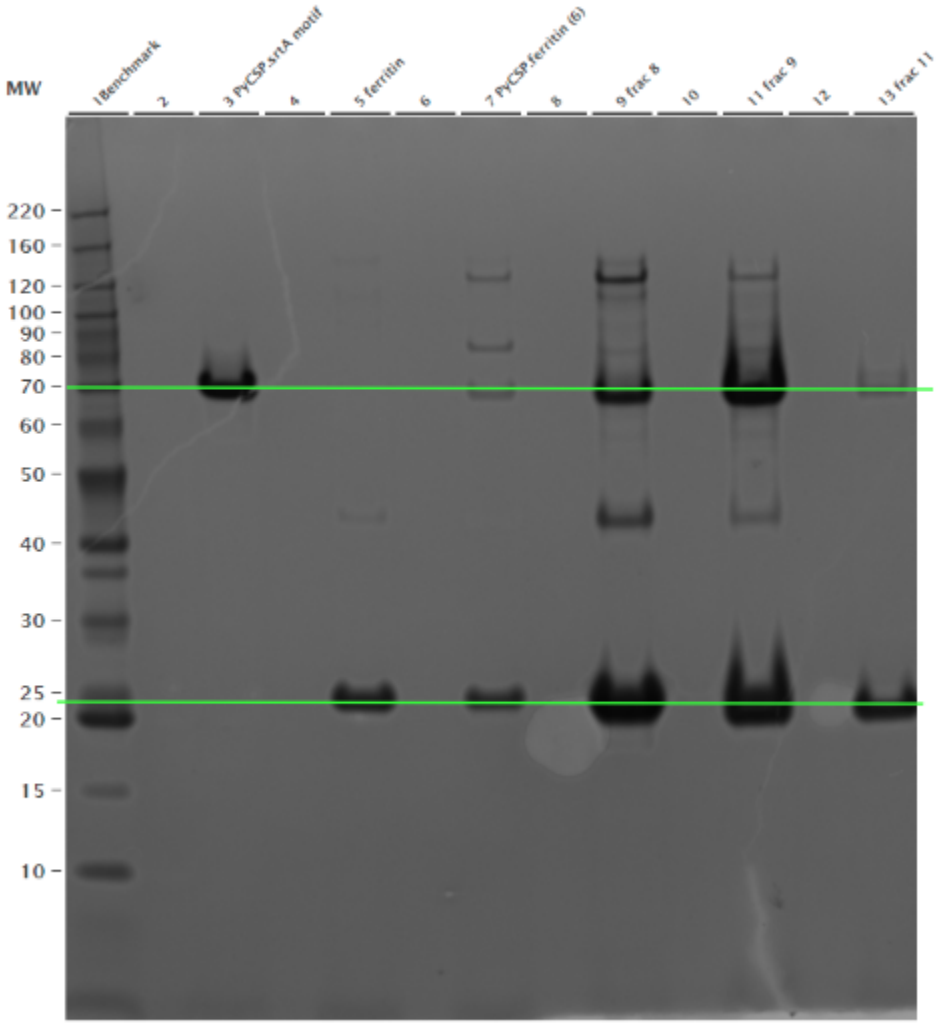

Figure 5: This SDS PAGE shows PyCSP and ferritin controls compared against a sortase A conjugation reaction after SEC was performed. SEC fractions from three different time points are shown. The highlighted bands represent PyCSP at ~70 kDa and ferritin at ~25 kDa.

As a result, optimization of the sortase A reaction was required to successfully conjugate ferritin. Multiple constructs were generated using site-directed mutagenesis, including an LPSTGG tag inserted at the end of the sequence, an LPSTGG at the end of the sequence with a GSGG linker, and an LPSTGG tag inserted between the PyCSP sequence and the histidine and avidin tags (His.Avi). Figure 6 shows a visual representation of the optimal sequence design.

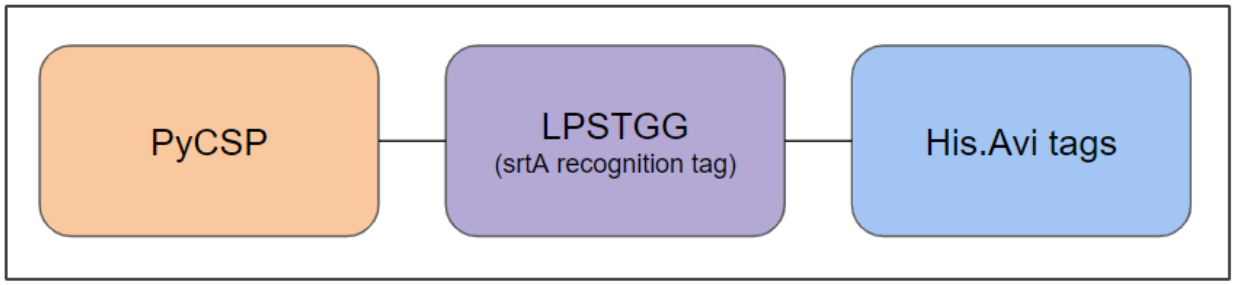

Figure 6: The optimal sequence design for the srtA-compatible PyCSP construct. The PyCSP is at the N terminus, followed by the LPSTGG tag positioned between the His.Avi tags at the C terminus and the PyCSP.

This configuration is believed to be optimal due to the mechanism of the srtA reaction, in which the srtA enzyme requires two sites to bind before cleaving the protein at the final glycine residue of the LPSTGG tag and joining it to the complementary pentaglycine tag located on the ferritin construct [21]. After optimizing the srtA reaction, conjugated PyCSP-ferritin nanoparticles were isolated using size-exclusion chromatography and verified by SDS PAGE. Figure 7 shows a successful conjugation.

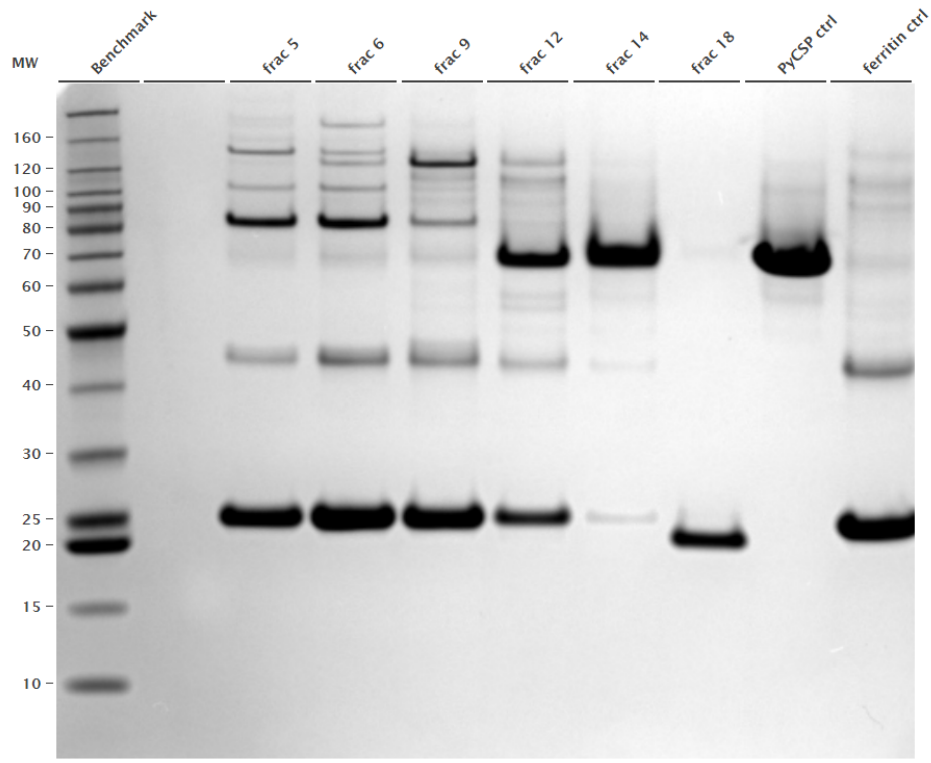

Figure 7: SDS PAGE data showing a successful ferritin conjugation. SEC fractions 5, 6, 9, 12, 14, and 18 were run in addition to PyCSP and ferritin controls. Fractions 5 and 6 show no presence of PyCSP, but do show presence of ferritin and another material which is roughly 90 kDa, or the expected size of PyCSP and ferritin together. This indicates that these samples contain nanoparticles consisting of both PyCSP-conjugated and unconjugated ferritin subunits.

The presence of both ~90 kDa bands and ~23 kDa bands in SEC fractions 5 and 6 indicate that these fractions contain nanoparticles consisting of conjugated and unconjugated ferritin subunits. The unpaired PyCSP can be seen in fractions 12 and 14. This is expected behavior for nanoparticle assembly; it is difficult to achieve full antigen decoration of a nanoparticle, especially with an antigen as large as PyCSP [18, 19]. With this information, it was determined that these PyCSP-ferritin nanoparticles were ready to be tested *in vivo* alongside the previously constructed heptamer and monomer forms of PyCSP.

Materials and Methods

Plasmids were designed *in silico* using the Geneious software and verified by restriction digest as described in detail above. Candidate designs included a PyCSP[NXA] plasmid with the LPSTGG tag inserted at the C terminal end of the coding sequence, an LPSTGG tag at the C terminus spaced by a GSGG linker sequence, and an LPSTGG tag inserted between the PyCSP coding sequence and the histidine tag.

HBS-E buffer was prepared with 10 mM HEPES (pH 7), 150 mM NaCl, and 2 mM EDTA.

All constructs were synthesized using the following site-directed mutagenesis protocol. 10 ng of the parent PyCSP[NXA] plasmid were mixed with 10 μM forward primer, 10 μM reverse primer, and 12.5 μL of Q5® High-Fidelity 2X Master Mix (NEB #M0492), and the reaction was filled to a total volume of 25 μL with molecular biology grade water. The reaction was then run in a thermocycler at 95C for 10s, 25 cycles comprising: 95C for 10s, 60C for 20s, 72C for 2.5min, and a final extension phase at 72C for 5min. 1 μL of *Dpn* I restriction enzyme (NEB #R017) was added to the reaction, and the reaction was incubated at 37C for 1 hour in the thermocycler. 2 μL of the reaction was then transformed into NEB 5-alpha C2987H cells and plated on antibiotic-treated agar plates. Colonies were then selected for extraction using miniprep and verified by Sanger sequencing.

Following verification of selected clones, the plasmids were then transfected into HEK 293F cells and purified by IMAC and SEC as described in detail above. Successful purification was verified by SDS PAGE and Western Blot.

After the successful addition of the LPSTGG C-terminal tag to PyCSP, conjugation with ferritin was confirmed. Reagents were mixed at a ratio of 10 μM LPSTGG-tagged PyCSP, 20 μM ferritin with an N-terminal penta-glycine tag (produced in-house) and 5 μM calcium-independent sortase A enzyme (produced in-house as previously described) [20]. The reaction was incubated at room temperature for 1 hour before purification by SEC. Successful nanoparticle formation was then verified by SDS PAGE.

IV. LIPOSOME SYNTHESIS

In the interest of generating nanoparticles capable of expressing higher amounts of antigen copies than the IMX313 or ferritin nanoparticles, liposomes were considered as another multimerization platform for PyCSP. Liposomes are small particles composed of a phospholipid bilayer surrounding an aqueous core, and have previously been used by the Sather lab to successfully conjugate HIV-1 envelope proteins for high-valency expression. Given that the PyCSP[NXA] construct being used in this study comprises a histidine tag, this would allow it to be conjugated to the surface of a liposome containing cobalt in its membrane.

Results and Discussion

Conjugation of PyCSP to liposomes was attempted twice, with little success either time. In the first instance, the liposomes failed to assemble, likely due to a contaminant in the sample. In the second instance, liposomes were produced; however, upon attempting to quantify the liposomes after performing SEC, it was concluded that the sample contained only trace amounts of conjugated liposomes that were insufficient for use in further studies, as seen in Figure 8.

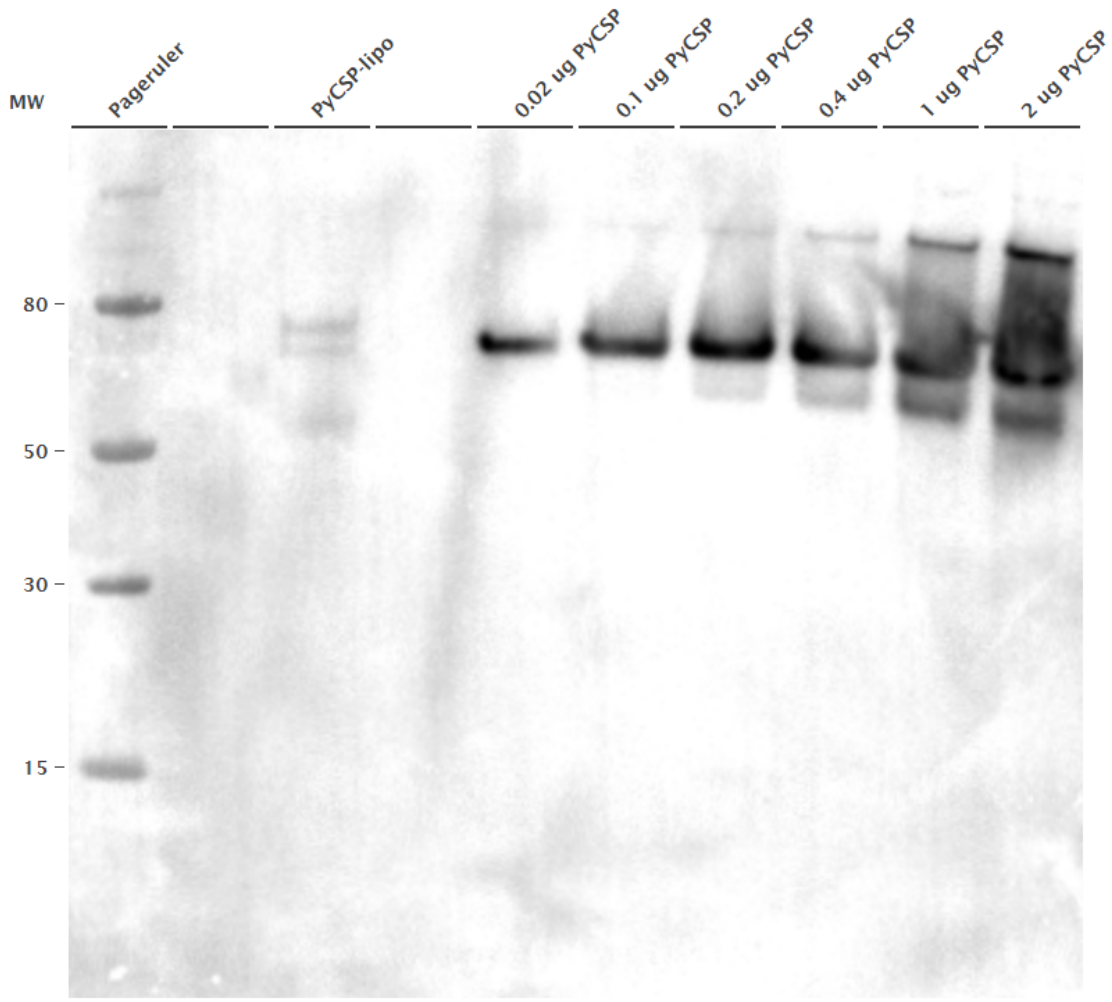

Figure 8: Quantitative western blot of conjugated liposome sample. The western blot was performed using the 2F6 antibody, an anti-PyCSP antibody. The conjugated liposome sample is shown in the third column, and contains trace amounts of PyCSP, even less than the 0.02 ug control sample.

Due to time constraints of the program timeline, optimization of the liposome conjugation was not pursued further. However, this could be an area of interest in future research. As stated previously, higher degrees of multimerization have shown improved immune responses when used for other pathogens, and liposomes could be a way to accomplish this with PyCSP.

Materials and Methods

Liposomes expressing PyCSP were synthesized according to the following protocol. 1,2-Dipalmitoyl-sn-glycero-3-phosphocholine (Sigma #P4329-25MG), Cholesterol (Sigma #C8667-500MG), 18:0 DGS-NTA(Co)1,2-dioleoyl-sn-glycero-3-[(N-(5-amino-1-carboxypentyl)iminodiacetic acid)succinyl] (Cobalt salt), Chloroform (Avanti Polar Lipids #791113P-5mg), and monophosphoryl lipid A (Avanti Polar Lipids #699800) were combined at a 50:36:4:5:5 ratio. Nitrogen gas was passed over the solution before it was left to desiccate overnight at room temperature in nitrogen gas. The mixture was then resuspended in 2mL of PBS, incubated in a shaker at 37C for 2 hours, sonicated in a water bath for 30 seconds, then extruded. The solution was then incubated with PyCSP[NXA] buffer-exchanged into PBS at room temperature for 2 hours to conjugate the recombinant PyCSP[NXA] to the NiNTA-bearing lipid surface. Liposome construction and PyCSP conjugation were verified by SEC and SDS PAGE.

V. IMMUNOGENICITY OF MULTIMERIZED PYCSP IN MICE TRIALS

Following successful construction of PyCSP nanoparticles, their immunogenicity was assessed *in vivo* using a murine model of immunization. BALB/cj mice were immunized with protein antigens and AddaS03 adjuvant, boosted, and blood samples collected to evaluate antibody titers. First, the PyCSP-IMX313 heptamer was compared against monomeric PyCSP using ELISA to detect antibody titers from blood samples. A later study compared PyCSP-IMX313 and PyCSP-ferritin particles, as well as a recombinant PyCSP[NXA] monomer.

Results and Discussion

To compare immunogenicity of antigens *in vivo*, the PyCSP-IMX313 heptamer was first compared against a recombinant PyCSP monomer control. First, antibody titers against total Ig

were compared between the two constructs as shown in Figure 9. While some individual mice showed higher antibody responses, an unpaired t test yielding a p value of 0.4036 indicates no statistical significance in these findings.

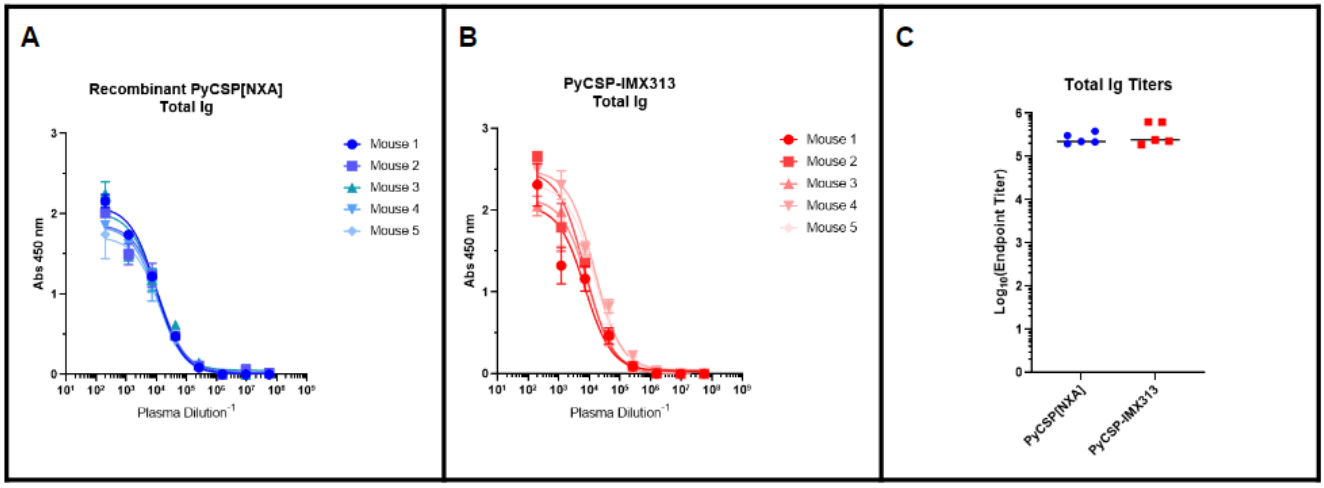

Figure 9: ELISA data comparing total Ig antibody response from mice immunized with PyCSP monomer (A) and PyCSP-IMX313 (B). Panel C shows a comparison of the total Ig titers between the two constructs.

Additionally, IgG1, IgG2a, IgG2b, and IgG3 antibody subclasses were compared between mice immunized with PyCSP monomers and heptamers as shown in Figures 10-13. Significance was again assessed by an unpaired t test. The IgG1 subclass had a $p = 0.4932$, IgG2a had $p = 0.7551$, IgG2b had $p = 0.2521$, and IgG3 had $p = 0.3053$. Therefore, there was no significant difference in antibody response in any subclass. However, as shown in Figures 10-13, certain individual mice exhibited higher antibody affinity for PyCSP[NXA], particularly in the IgG2a and IgG2b subclasses.

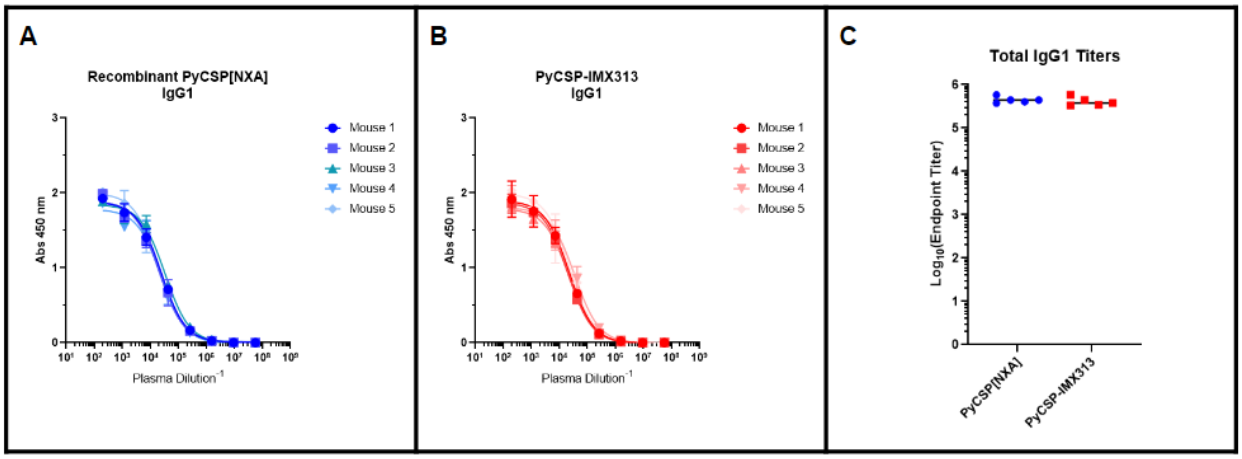

Figure 10: ELISA data comparing IgG1 subclass antibody response from mice immunized with PyCSP monomer (A) and PyCSP-IMX313 (B). Panel C shows a comparison of the total IgG1 titers between the two constructs.

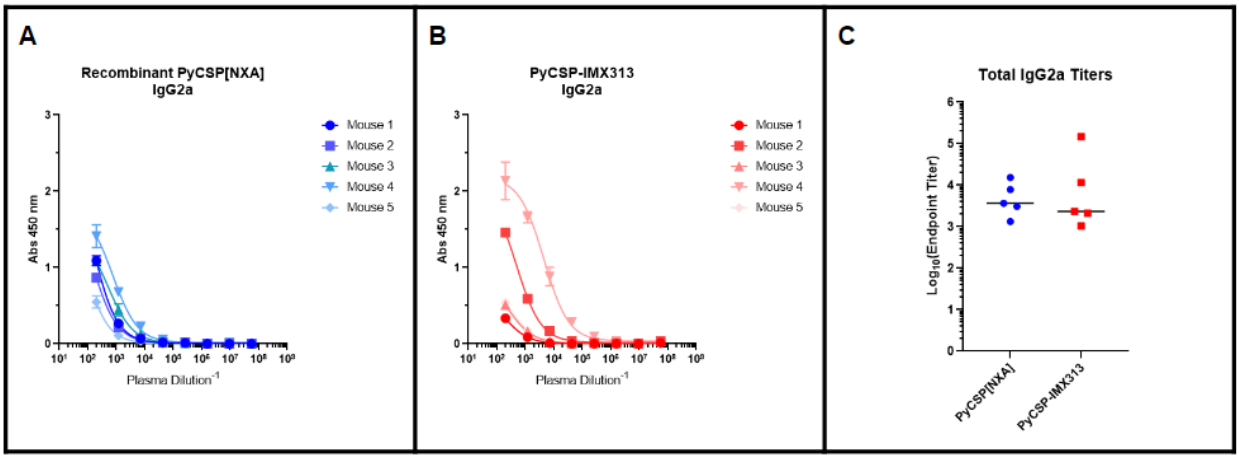

Figure 11: ELISA data comparing IgG2a subclass antibody response from mice immunized with PyCSP monomer (A) and PyCSP-IMX313 (B). Panel C shows a comparison of the total IgG2a titers between the two constructs.

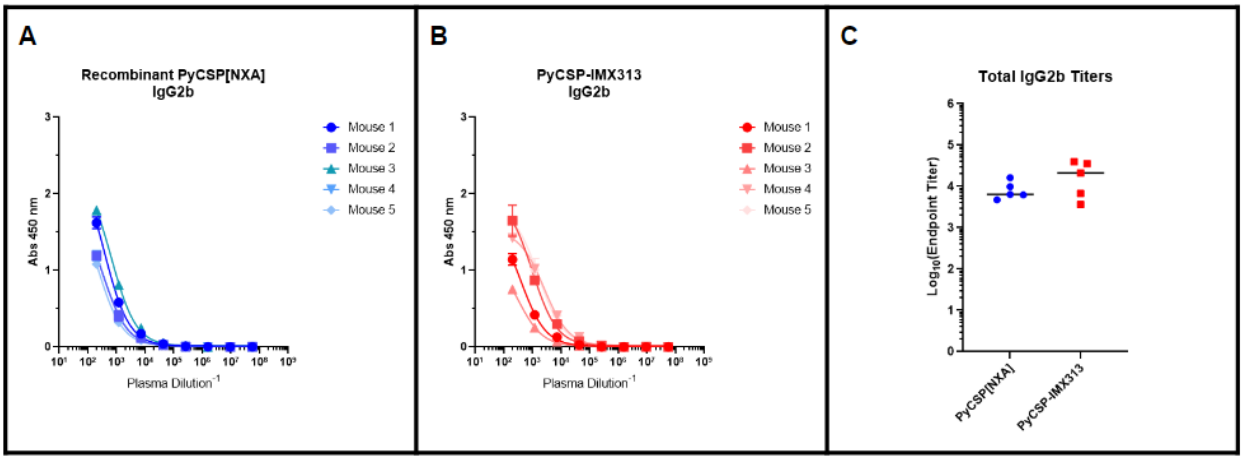

Figure 12: ELISA data comparing IgG2b subclass antibody response from mice immunized with PyCSP monomer (A) and PyCSP-IMX313 (B). Panel C shows a comparison of the total IgG2b titers between the two constructs.

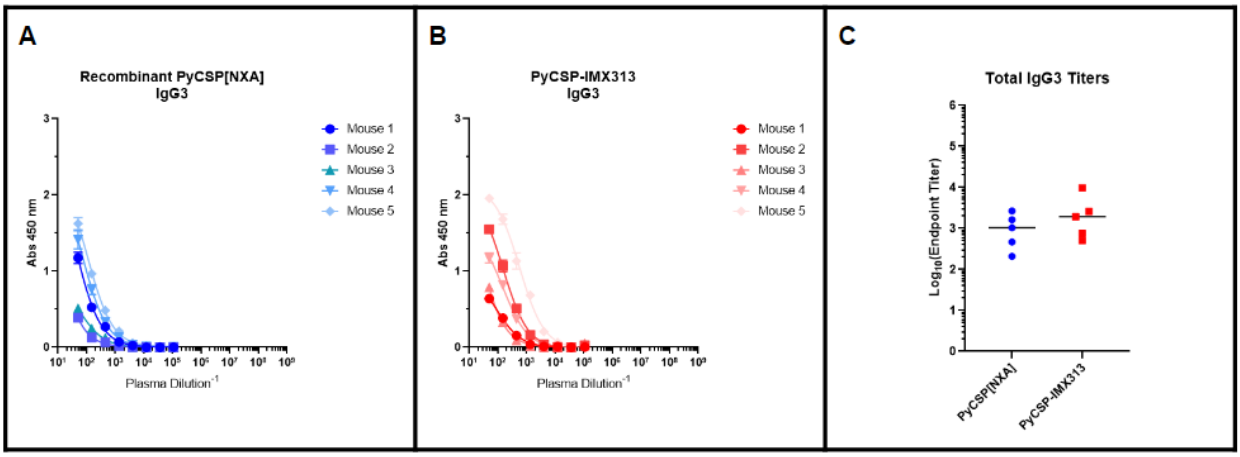

Figure 13: ELISA data comparing IgG3 subclass antibody response from mice immunized with PyCSP monomer (A) and PyCSP-IMX313 (B). Panel C shows a comparison of the total IgG3 titers between the two constructs.

Finally, binding avidity was compared between the PyCSP monomer and heptamer as shown in Figure 14. When comparing the avidity index of the two constructs, the value $p = 0.4428$ after performing an unpaired t test indicates no statistically significant difference between the binding avidity of antibodies elicited by the monomer in comparison to the heptamer.

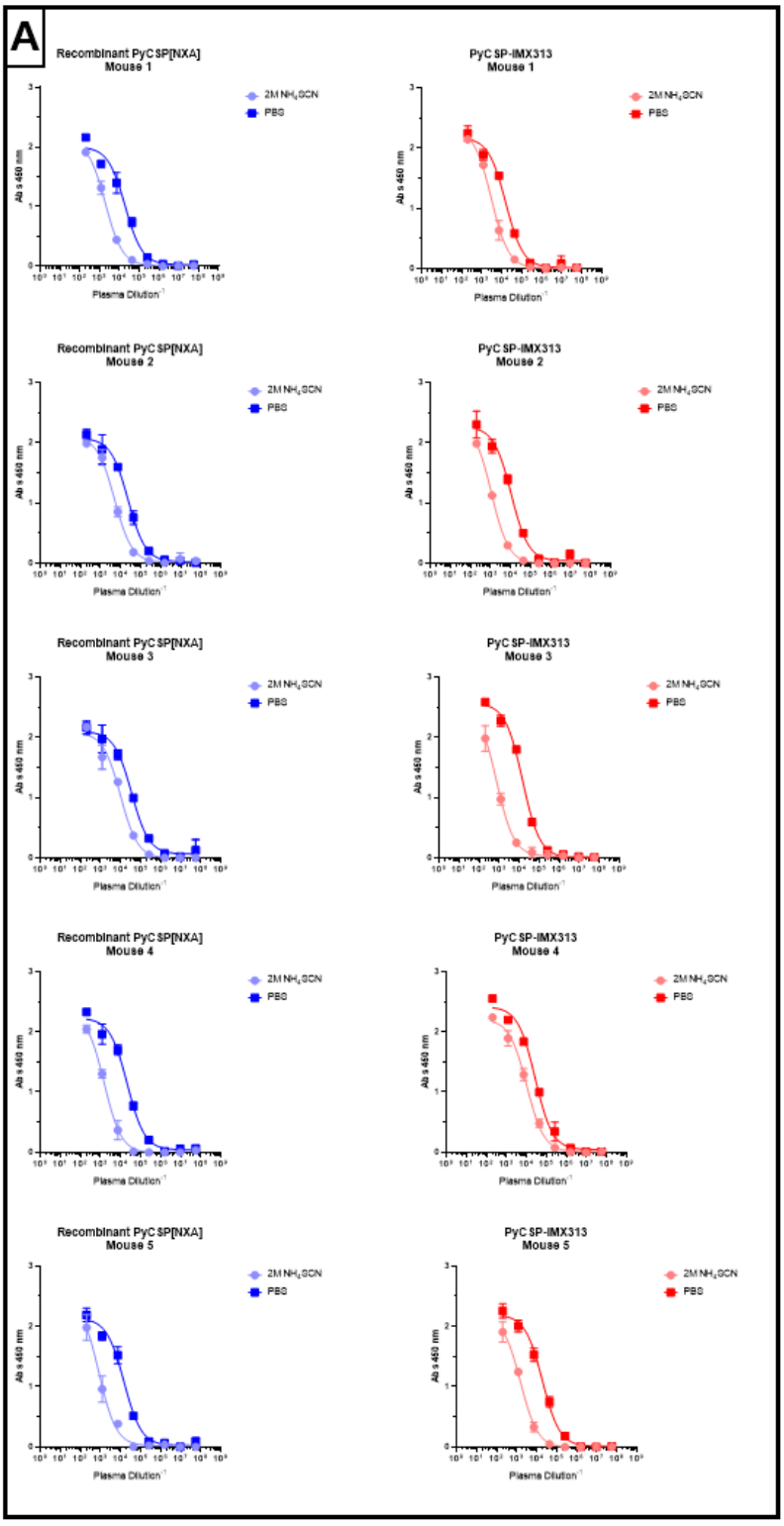
A
Recombinant PyC SP[NXA]
Mouse 1
PyC SP-IMX313
Mouse 1
Recombinant PyC SP[NXA]
Mouse 2
PyC SP-IMX313
Mouse 2
Recombinant PyC SP[NXA]
Mouse 3
PyC SP-IMX313
Mouse 3
Recombinant PyC SP[NXA]
Mouse 4
PyC SP-IMX313
Mouse 4
Recombinant PyC SP[NXA]
Mouse 5
PyC SP-IMX313
Mouse 5
2M NH4SCN
PBS
Ab s 450 nm
Plasma Dilution-1

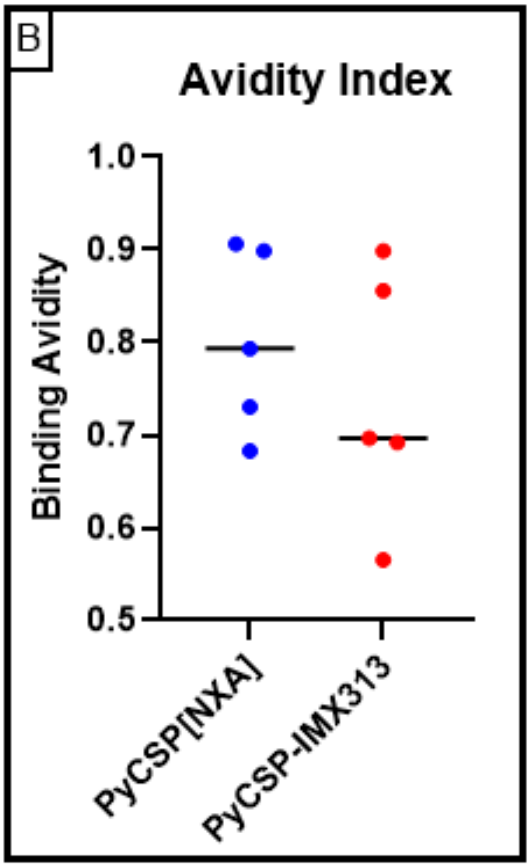

Figure 14: Panel A shows a compilation of plots comparing individual mouse samples when treated with NH_4SCN vs. a PBS control. Panel B shows a comparison between the avidity index of antibodies elicited by monomeric vs. heptameric PyCSP.

While the initial study did not show a statistically significant improvement in antibody response between the monomer and heptamer, unanswered questions remained. PyCSP is known to generate high antibody titers on its own when used at high concentrations, so the antigen could have been overloaded, making comparison between these two constructs difficult to distinguish. Additionally, the IMX313 heptamer is relatively small in comparison to other nanoparticles. As a result, a second *in vivo* study was designed to address these shortcomings. In the second study, PyCSP-ferritin nanoparticles generated by the srtA method were included; ferritin nanoparticles can bind up to 24 substrates if fully decorated. Additionally, 7 ug of antigen was injected per

mouse rather than the initial 20 ug to allow for a more distinguishable comparison of antibody titers.

However, the results from the second *in vivo* study did not align with this hypothesis. With a lower dose of antigen, there was still no statistically significant difference in antibody titers between the PyCSP monomer and the PyCSP-IMX313 heptamer. Interestingly, despite being the largest nanoparticle tested, mice injected with PyCSP-ferritin nanoparticles generally displayed lower antibody titers.

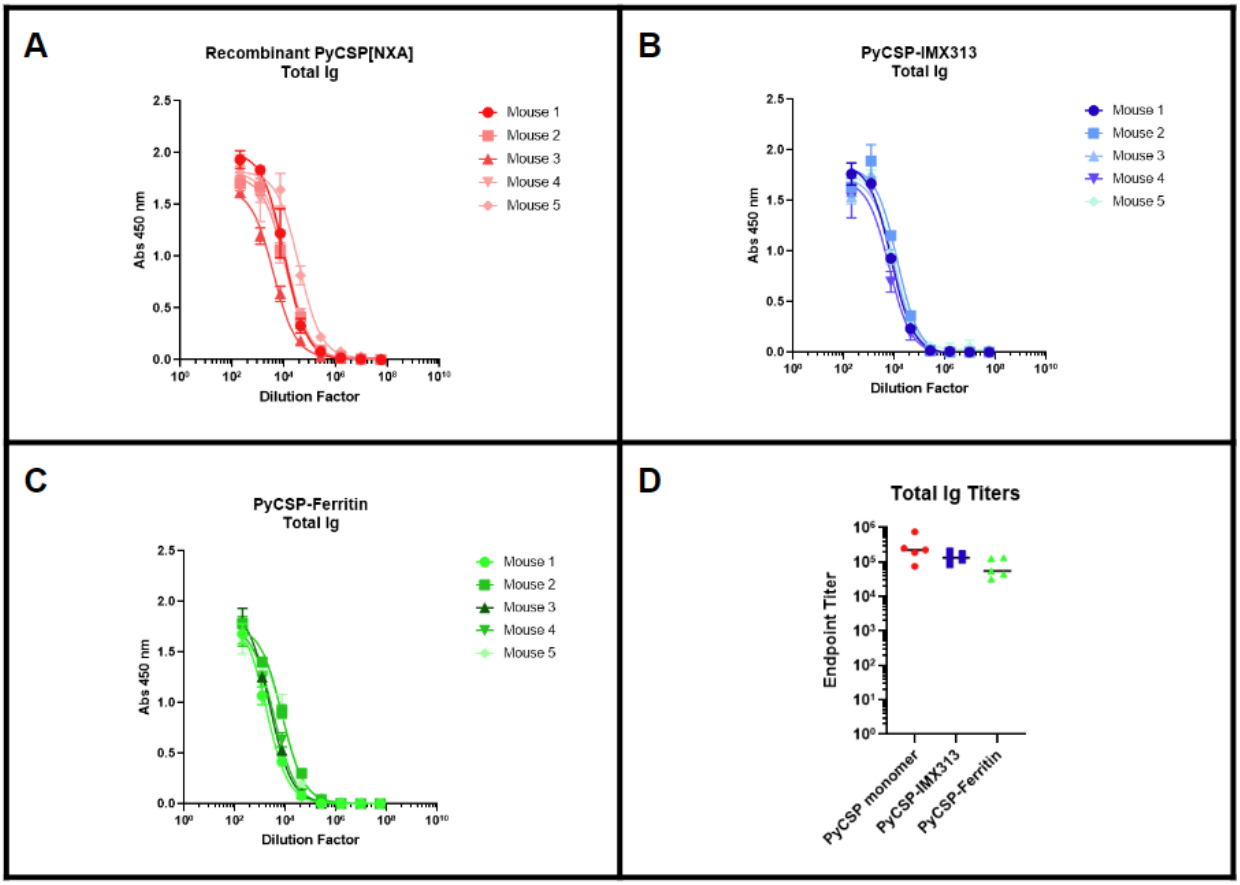

Figure 15: ELISA data comparing total Ig antibody response from mice immunized with PyCSP monomer (A), PyCSP-IMX313 (B), and PyCSP-ferritin (C). D shows a comparison of the total Ig titers between the three constructs.

As shown in Figure 15, the total Ig response at week 4 does not show a significant difference in antibody titers between PyCSP monomer and PyCSP-IMX313 (p=0.2370). However, PyCSP-ferritin shows significantly lower antibody titers when compared to monomeric PyCSP (p=0.0302). This trend was also seen in the subclass and avidity ELISAs shown in Figures 16-20.

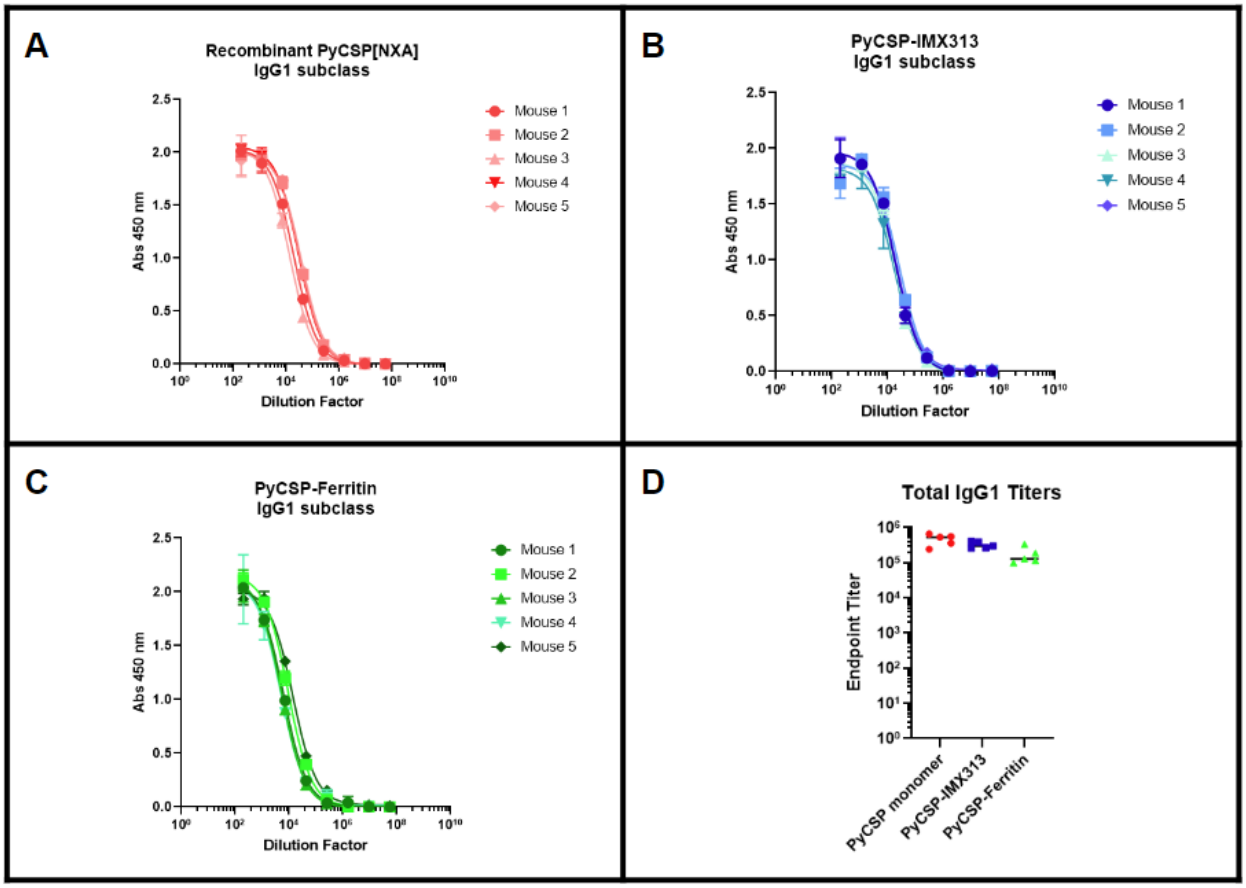

Figure 16: ELISA data comparing IgG1 subclass antibody response from mice immunized with PyCSP monomer (A), PyCSP-IMX313 (B), and PyCSP-ferritin (C). D shows a comparison of the IgG1 titers between the three constructs.

As shown in Figure 16, the IgG1 response at week 4 does not show a significant difference in antibody titers between PyCSP monomer and PyCSP-IMX313 (p=0.1430). However, PyCSP-ferritin shows significantly lower antibody titers when compared to monomeric PyCSP (p=0.0057).

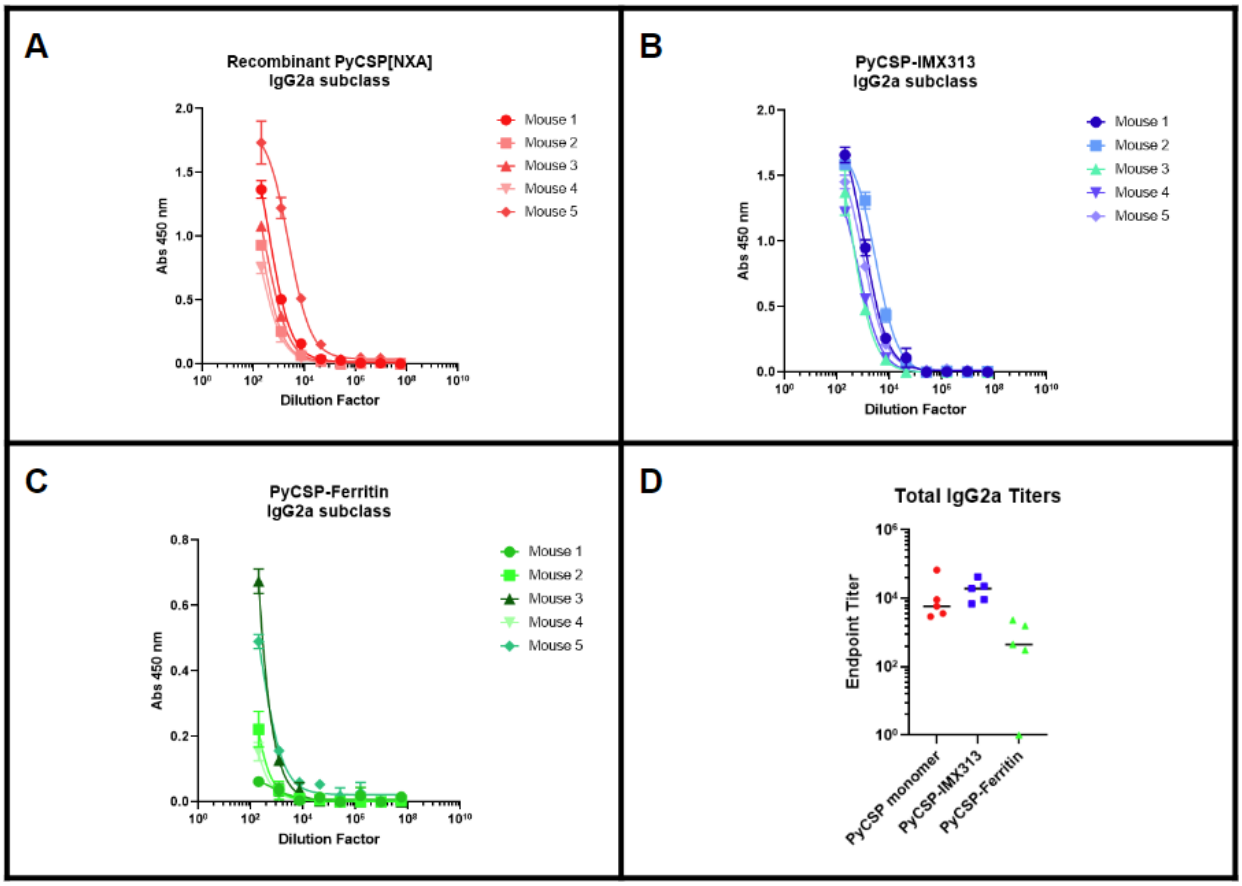

Figure 17: ELISA data comparing IgG2a subclass antibody response from mice immunized with PyCSP monomer (A), PyCSP-IMX313 (B), and PyCSP-ferritin (C). D shows a comparison of the IgG2a titers between the three constructs.

As shown in Figure 17, the IgG2a response at week 4 does not show a significant difference in antibody titers between PyCSP monomer and PyCSP-IMX313 ($p=0.3217$). However, PyCSP-ferritin shows significantly lower antibody titers when compared to monomeric PyCSP ($p=0.0423$).

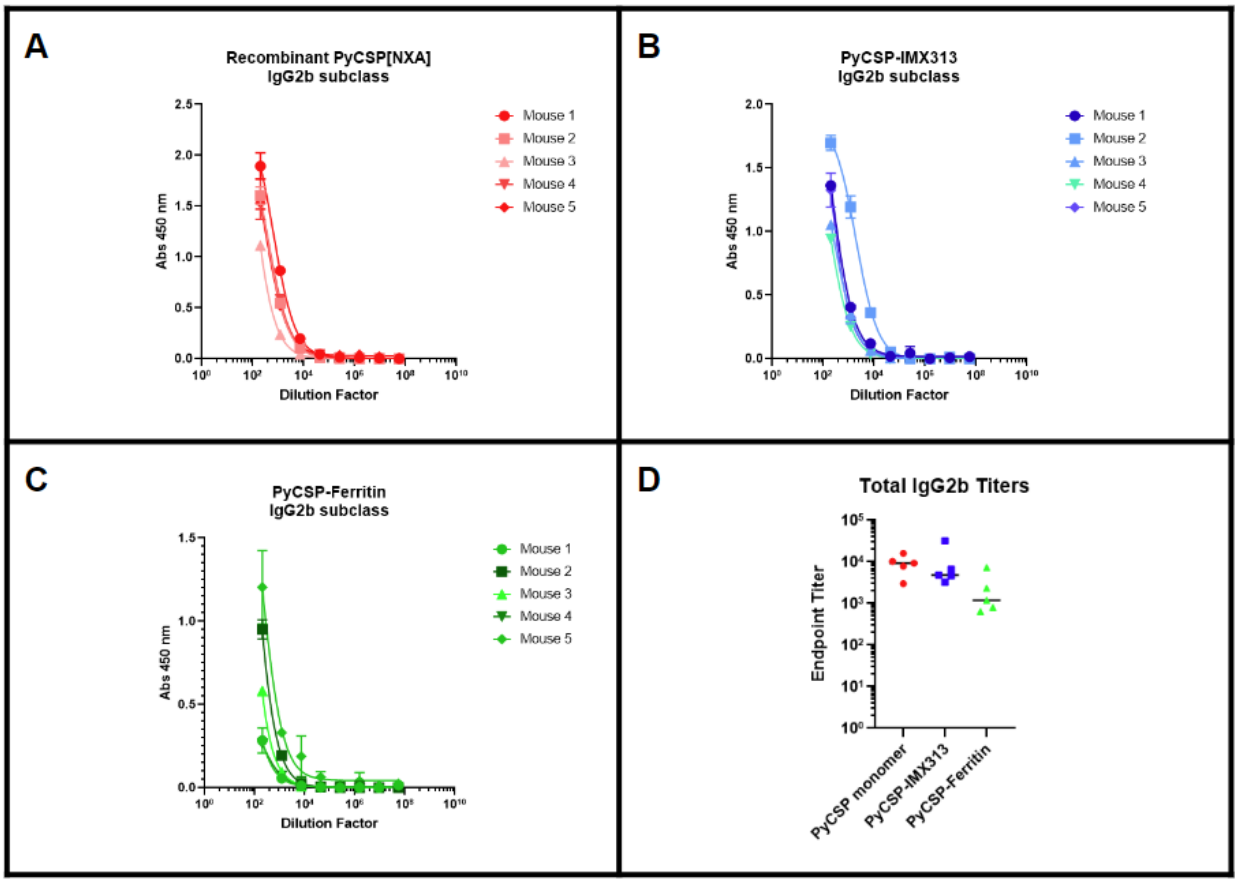

Figure 18: ELISA data comparing IgG2b subclass antibody response from mice immunized with PyCSP monomer (A), PyCSP-IMX313 (B), and PyCSP-ferritin (C). D shows a comparison of the IgG2b titers between the three constructs.

As shown in Figure 18, the IgG2b response at week 4 does not show a significant difference in antibody titers between PyCSP monomer and PyCSP-IMX313 ($p=0.7361$). However, PyCSP-ferritin shows significantly lower antibody titers when compared to monomeric PyCSP ($p=0.0138$).

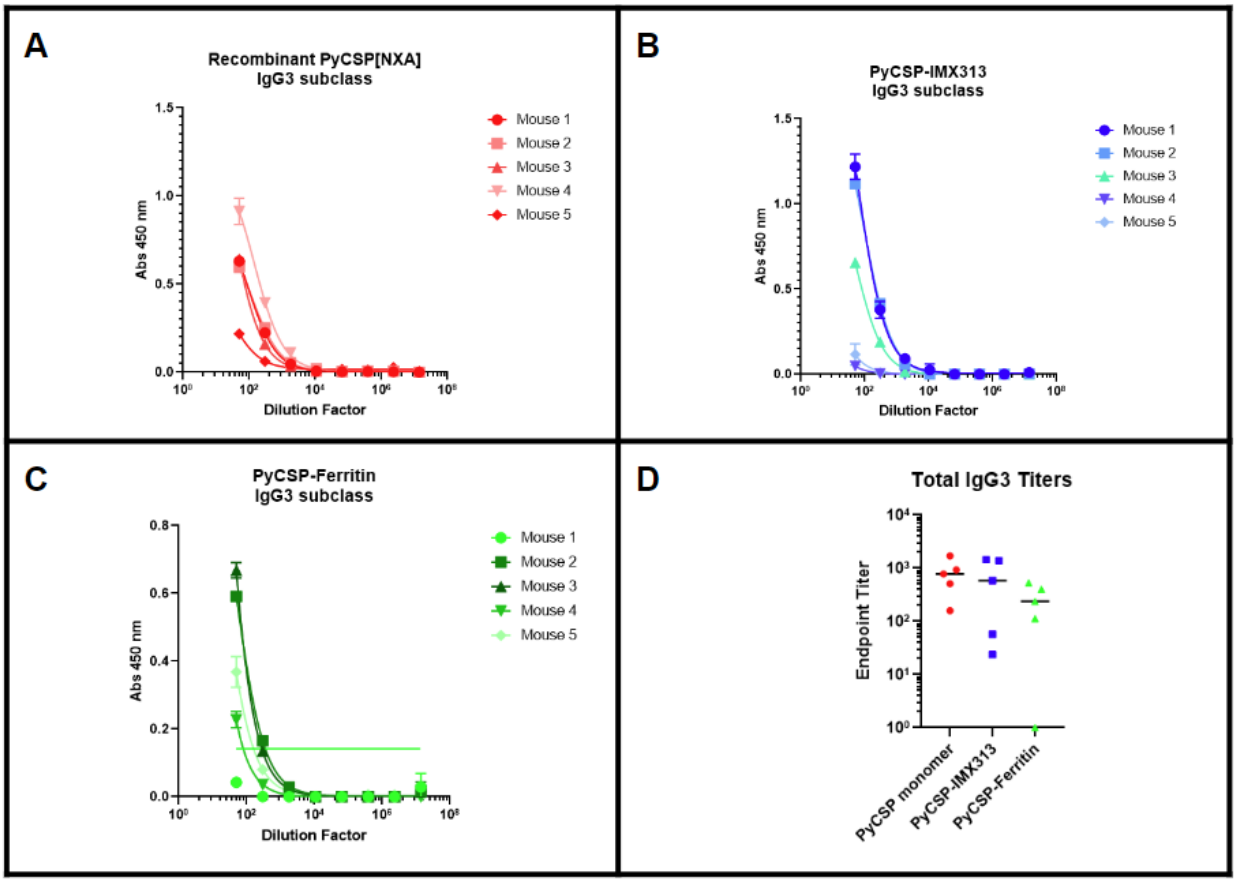

Figure 19: ELISA data comparing IgG3 subclass antibody response from mice immunized with PyCSP monomer (A), PyCSP-IMX313 (B), and PyCSP-ferritin (C). D shows a comparison of the IgG3 titers between the three constructs.

As shown in Figure 19, the IgG3 response at week 4 does not show a significant difference in antibody titers between PyCSP monomer and PyCSP-IMX313 ($p=0.4032$). PyCSP-ferritin also shows no significant difference when compared to monomeric PyCSP ($p=0.1471$).

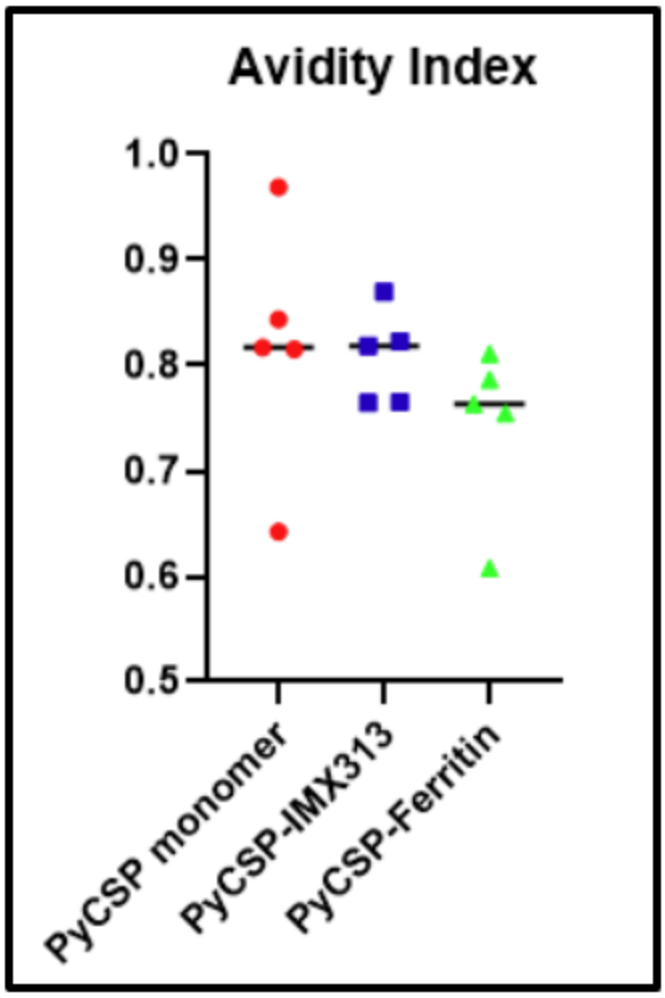

Figure 20: Comparison between the avidity index of antibodies elicited by monomeric PyCSP, PyCSP-IMX313, and PyCSP-ferritin.

As shown by Figure 20, the avidity of the antibody response showed no statistically significant difference between constructs. A p value of 0.8721 was obtained from an unpaired t test comparing the PyCSP monomer and PyCSP-IMX313, and a p value of 0.2821 was obtained from an unpaired t test comparing the PyCSP monomer and PyCSP-ferritin.

In order to better explain these results, an anti-ferritin ELISA was performed to test if the mice had developed an immune response against ferritin.

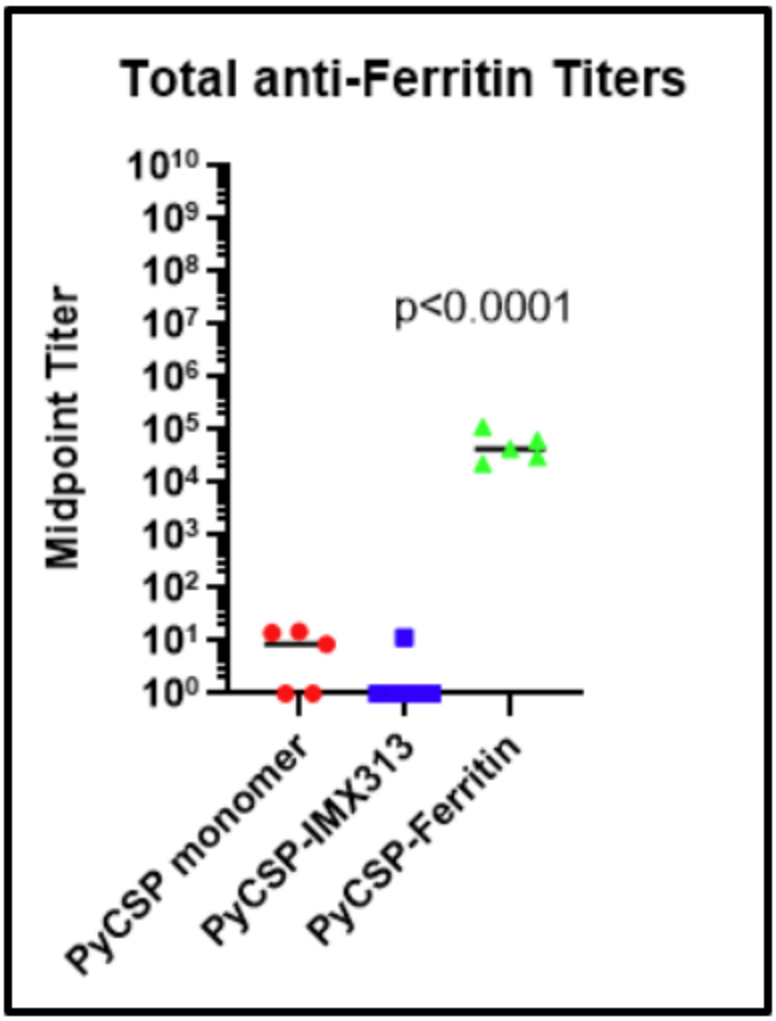

Figure 21: Comparison of total Ig titers against ferritin for mice immunized with PyCSP monomer, PyCSP-IMX313, and PyCSP-ferritin. The p value was determined from an unpaired t test.

Figure 21 summarizes these results, showing that while mice immunized with PyCSP monomer and PyCSP-IMX313 display little to no antibody response against ferritin, mice immunized with PyCSP-ferritin exhibit a significant response ($p<0.0001$). This shows that the ferritin scaffold used was immunogenic itself, and likely competed with the displayed PyCSP antigen, dampening the anti-PyCSP response. This would explain why despite being a larger particle, the PyCSP-ferritin nanoparticles overall displayed lower antibody antibody titers for PyCSP.

However, despite lower overall antibody antibody titers, another key difference between PyCSP-ferritin nanoparticles and the other constructs was observed. When comparing total Ig titers between the bleeds at weeks 3 and 4, PyCSP-ferritin was the only construct to see a significant increase in antibody titers.

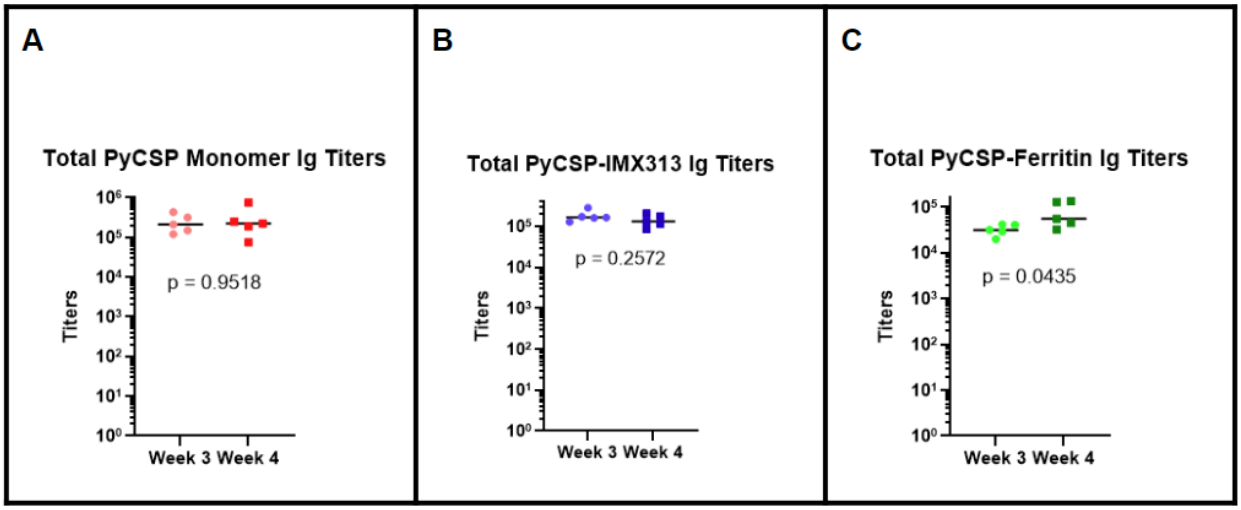

Figure 22: Comparison of total Ig titers at between the week 3 and week 4 bleeds for PyCSP monomer (A), PyCSP-IMX313 (B), and PyCSP-ferritin (C). P values were determined by unpaired t test.

As shown in Figure 22, there is no significant difference in titers between weeks 3 and 4 for both PyCSP monomer and PyCSP-IMX313 ($p=0.9518$ and $p=0.2572$, respectively). However, there is a statistically significant increase in titers between time points for PyCSP-ferritin ($p=0.0435$). This result is further supported by the literature, in which nanoparticle size has been shown to influence the retention of antigens within lymph nodes, with larger particles being retained longer [22]. This suggests that the increase in PyCSP-ferritin antibody titers at week 4 could be due to the particles being retained longer in germinal centers such as lymph nodes, resulting in a delayed immune response against PyCSP. Advantageously, this could allow for a more sustained immune response against malaria.

Materials and Methods

BALB/cj mice were used in this study to determine which multimer configuration elicits the optimal immune response. In the initial study comparing PyCSP-IMX313 with the monomer, animals were immunized with 20 ug of antigen each two times at weeks 0 and 2 with the AddaS03 adjuvant, and blood harvested by submandibular bleed at week 3. A subsequent study with 7 ug of antigen per mouse was performed along with the addition of the ferritin construct. Blood samples were harvested by submandibular bleed at week 3 and the animals were euthanized and then exsanguinated at week 4. Vaccine-elicited antibodies were assessed using parameters such as antibody binding titers to CSP proteins, avidity of polyclonal antibodies, and distribution of IgG subclass. These parameters were measured by direct ELISA in a 96-well Immlon 2HB flat bottom polystyrene microtiter plate (ThermoScientific, #3455) by coating wells with PyCSP[NXA] diluted in 0.1M sodium bicarbonate at a concentration of 0.5 ng/uL overnight and blocked using non-fat milk blocking buffer (10% non-fat milk in PBS, 0.3% Tween-20). All antibody and plasma samples were diluted in non-fat milk dilution buffer (10% non-fat milk in PBS, 0.03% Tween-20). Prior to analysis, blood samples were heat-inactivated at 56C for 30 minutes before being centrifuged at 17,000 g for 10 minutes.

The total Ig ELISAs were performed with a starting sample dilution of 1:200. The antibody 2F6 was used as a positive control at a starting concentration of 1 ng/uL. A six fold serial dilution was then performed. The HRP-conjugated secondary antibody Goat Anti-Mouse Ig (Southern Biotech #1013-05) was used at a 1:2000 dilution. Endpoint absorbance was measured at 450 nm. An additional anti-ferritin ELISA was performed according to the same protocol by coating

wells with GGG-ferritin rather than PyCSP[NXA] diluted in 0.1M sodium bicarbonate at a concentration of 0.5 ng/uL overnight.

The avidity ELISAs were performed with a starting sample dilution of 1:200. A six fold serial dilution was then performed. After the primary antibody incubation, every other well was treated with 100 uL of either PBS (untreated control) or 2M NH_4SCN for 20 minutes at room temperature to disrupt binding. The HRP-conjugated secondary antibody IgG-Fc Goat Anti-Mouse (Southern Biotech #1033-05) was used at a 1:2000 dilution. Absorbance was measured at 450 nm to derive the endpoint titer, meaning the highest dilution at which antibody binding can be detected

The IgG1 subclass ELISAs were performed with a starting sample dilution of 1:200. The antibody 2F6 was used as a positive control at a starting concentration of 1 ng/uL. A six fold serial dilution was then performed. The HRP-conjugated secondary antibody IgG1 Goat Anti-Mouse (Southern Biotech #1071-05) was used at a 1:4000 dilution. Endpoint absorbance was measured at 450 nm.

The IgG2a and IgG2b subclass ELISAs were performed with a starting sample dilution of 1:200. Pooled mouse plasma samples reactive to PyCSP were used as a positive control at a starting dilution of 1:200. A six fold serial dilution was then performed, titrating from 1:200 to 55,987,200. The HRP-conjugated secondary antibodies IgG2a and IgG2b Goat Anti-Mouse (Southern Biotech #1081-05, #1091-05) were used at a 1:4000 dilution. Endpoint absorbance was measured at 450 nm.

The IgG3 subclass ELISAs were performed with a starting sample dilution of 1:50. Pooled mouse plasma samples reactive to PyCSP were used as a positive control at a starting dilution of 1:50. A three fold serial dilution was then performed. The HRP-conjugated secondary antibody IgG3 Goat Anti-Mouse (Southern Biotech #1101-05) was used at a 1:4000 dilution. Endpoint absorbance was measured at 450 nm.

For the total Ig and subclass ELISAs, data was processed by subtracting average plate background (calculated from blank wells) from all sample wells and inputting into Graphpad Prism. Data was plotted by transforming the dilution factor with a x = log(x) transformation. Afterwards, the data was fitted with a three-parameter nonlinear curve [log(agonist) vs. response]. Endpoint titers were determined as the dilution factor interpolated for an absorbance 450 of 0.1 using the non-linear curve. The significance in the difference between monomer and heptamer values was evaluated using an unpaired t test.

For the avidity ELISAs, the data was plotted as above, but area under the curve was used after applying the function x = 1/x to the dilution factor. The avidity index (ratio of the treated vs. untreated areas under the curves) was reported. The significance in the difference between these values was again evaluated using an unpaired t test.

VI. PARTIAL PYCSP CONSTRUCTS

The large size of PyCSP is believed to inhibit its ability to form nanoparticles. As shown previously in this study, efforts to synthesize larger nanoparticles using full-length PyCSP were

largely unsuccessful. While the use of the sortase A catalyzed reaction did result in successfully-assembled ferritin nanoparticles expressing PyCSP, only incomplete decoration of the particles was shown (Figure 7). Similarly to the failure of the genetic fusion methods, the size and shape of PyCSP could limit the number of antigen copies able to conjugate to the nanoparticle due to steric hindrance. To address this issue, ferritin nanoparticles expressing PyCSP deletion constructs were synthesized to test if greater conjugation efficiency could be achieved with smaller antigens.

Results and Discussion

Three PyCSP deletion constructs that have been previously characterized were modified with srtA recognition tags [23]. The deletion constructs used were: PyCSP[deltaN], a fragment of PyCSP with its N-terminal region removed, PyCSP[deltaC], a fragment of PyCSP with its C-terminal region removed, and PyCSP[N2rC], a fragment containing both N and C termini connected by two central repeat regions [23]. In addition to having the advantage of being smaller than full-length PyCSP, it is possible that fragment choice could influence the immune response due to the differing functionality of these regions of PyCSP at different points of the sporozoite's life cycle as it travels to the liver [23].

Following the design of these deletion constructs and subsequent expression in mammalian cells, they were conjugated to ferritin nanoparticles using the same srtA-mediated reaction as the full-length PyCSP construct. Figure 23 shows an SDS PAGE representing successful conjugation of the N2rC deletion construct to ferritin. However, like full-length PyCSP, there is evidence of

incomplete conjugation and the relative conjugation efficiencies of these constructs cannot be determined from SDS PAGE alone.

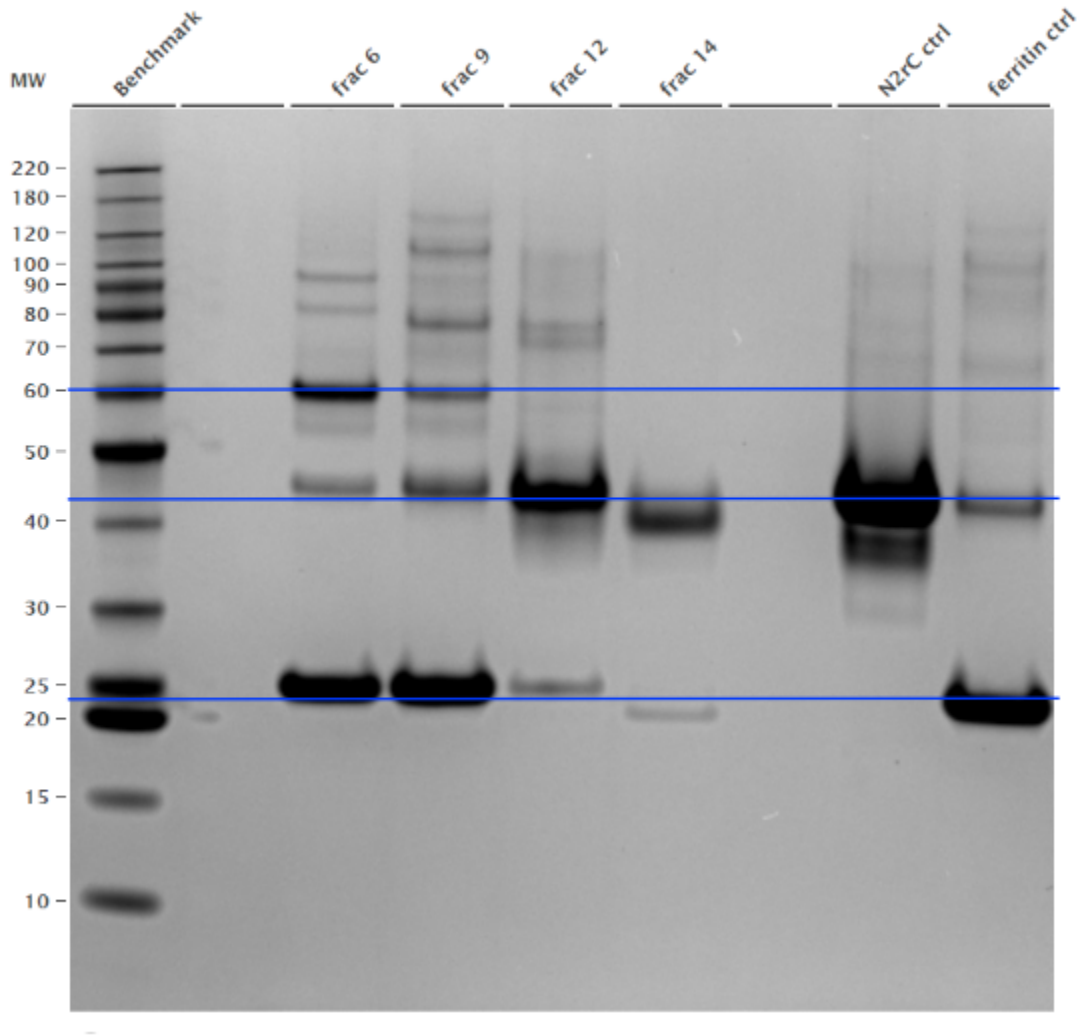

Figure 23: SDS PAGE data showing SEC fractions of a sortase A-mediated N2rC-ferritin conjugation. The bottom two bands show the control molecular weights of ferritin and PyCSP, and the top band shows the conjugated subunits present in fraction 6.

To further characterize these particles, they were measured using dynamic light scattering (DLS) alongside ferritin nanoparticles conjugated to full-length PyCSP.

Sample	Average Diameter	Polydispersity Index (PDI)
Full-length PyCSP	18.75 nm	0.03
PyCSP[N2rC]	18.51 nm	0.011
PyCSP[deltaN]	19.18 nm	0.032
PyCSP[deltaC]	21.04 nm	0.01

Table 1: Comparison of average particle diameter and PDI of ferritin nanoparticles expressing the three deletion constructs and full-length PyCSP. Data was obtained using DLS.

As shown in Table 1, all four particles have a polydispersity index (PDI) less than 0.2, indicating uniformity and successful assembly in the samples. This is advantageous for use in vaccine antigens because it replicates the appearance of a wild-type antigen and demonstrates stability.

In order to estimate the conjugation efficiency of each construct, unconjugated monomers of each PyCSP deletion construct were also measured by DLS. However, these proteins all showed a PDI > 0.2, meaning that they are too irregular in shape to accurately measure. As a result, the exact number of PyCSP antigens bound to each ferritin nanoparticle cannot be accurately estimated.

However, the average diameters of the PyCSP-ferritin nanoparticles measured can give some indication of this. As shown in the literature, an undecorated ferritin nanoparticle has a diameter of about 12 nm [24]. Table 1 shows that all conjugated ferritin nanoparticles have larger diameters, ranging from ~18 to 21 nm. With the exception of PyCSP[N2rC], all of the ferritin nanoparticles conjugated to deletion constructs are larger than the particles conjugated to full-length PyCSP. It is also worth noting that full-length PyCSP has a molecular weight of about

42 kDa, while the deletion constructs are smaller. PyCSP[deltaN] is about 33 kDa, PyCSP[deltaC] is about 31 kDa, and PyCSP[N2rC] is the smallest at about 25 kDa.

While more data is needed to formulate a more complete interpretation of the relative conjugation efficiencies, this information can be used to make some inferences. Given the larger sizes of the PyCSP deletion construct particles and their smaller size relative to full-length PyCSP, it is possible that the deletion constructs may conjugate more efficiently to ferritin, thereby achieving greater surface decoration, but more data is needed to draw a definitive conclusion. However, the uniformity of the samples does show evidence of uniformly decorated particles.

Materials and Methods

Plasmid vectors expressing each deletion construct (PyCSP[N2rC], PyCSP[deltaN], PyCSP[deltaC]) were modified with a C-terminal LPSTGG tag by site-directed mutagenesis as described in detail above. The LPSTGG tag was again inserted between the coding sequence of the protein and the His.Avi tags to optimize srtA-mediated conjugation. Sanger sequencing was then used to verify successful plasmid construction.

Plasmids were then transfected into HEK 293F cells and harvested as described above. Proteins were then purified using IMAC and SEC and verified by SDS PAGE. Purified proteins were then coupled to ferritin nanoparticles using the same protocol described above. Nanoparticles were then purified by SEC and successful coupling was verified by SDS PAGE.

All molecular weights referenced were estimated using the Geneious software based on amino acid sequences.

VII. CONCLUSION

While this study shows promising results for the use of protein nanoparticle vaccine antigens, more data is needed to fully optimize the beneficial effects shown. The longer retention time of larger particles in germinal centers could be studied over longer time courses in future *in vivo* studies, and other strategies could be used to make PyCSP-ferritin more immunogenic. For example, introducing non-native glycosylation sites to ferritin monomers has been shown to reduce immune responses against ferritin through glycan shielding after particle assembly, thereby enhancing the immune response against the conjugated antigen [25]. The addition of this modification to the PyCSP-ferritin construct could allow it to retain its long-acting effect while also generating higher anti-PyCSP antibody titers.

In order to better assess the conjugation efficiency of the nanoparticles, in particular the relative conjugation efficiencies of full-length PyCSP nanoparticles compared to nanoparticles comprising PyCSP deletion constructs, it would be necessary to measure these particles with more precision. One method that could help accomplish this is performing mass spectrometry on the nanoparticles. Given that the molecular weight of the nanoparticle itself and the conjugated antigens can be estimated based on amino acid sequence, the molecular weight of the assembled particle could be used to estimate how many antigen copies are conjugated to the particle. While this study did use DLS to measure the hydrodynamic diameters of these particles, this cannot be translated to molecular weight due to the complex secondary and tertiary structure of proteins.

Therefore, different techniques are needed to accurately make these measurements. One such method could be using a quantitative Western blot to measure the ratio of conjugated to unconjugated ferritin present in a sample.

Furthermore, optimizing the conjugation efficiency could provide more effective vaccine antigens. This would result in larger nanoparticles expressing more antigen copies. While this study suggests that deletion constructs of PyCSP could conjugate more efficiently to ferritin through a srtA-mediated reaction than full-length PyCSP, more data is needed to verify this. Additionally, the srtA-mediated conjugation system and PyCSP deletion constructs could be applied to other platforms that were previously unsuccessful in genetic fusion methods, such as lumazine synthase.

Additionally, these deletion constructs would need to be tested using *in vivo* studies; as shown in previous studies, different regions of PyCSP can result in different antibody responses [23]. PyCSP is a large and complex target, and the use of deletion constructs in combination with the present nanoparticle platforms could result in a more robust immune response against malaria.

Further characterization of these nanoparticle constructs are needed before they are ready to be used as vaccine antigens, but the data from this study shows they have the potential to address some of the current shortcomings of malaria vaccines. The longer-acting, sustained immune response resulting from longer germinal center retention of vaccine antigens could reduce the need for multiple injections, which are impractical in low-resource settings. Additionally, the use of protein nanoparticles expressing multiple copies of CSP deletion constructs has the potential

to generate a robust, long-acting, and targeted immune response, in addition to being durable and non-pathogenic antigens.

ACKNOWLEDGEMENTS

I would like to acknowledge the following people for assistance with this project: Dr. Noah Sather as the Principal Investigator and primary advisor, Dr. Danial Ratner as the bioengineering co-advisor, Dr. Vladimir Vigdorovich for molecular biology expertise and techniques, Mr. Nicholas Dambrauskas as the lab manager and assistance with laboratory techniques, Mr. Andrew Raappana for assistance with research and laboratory techniques, Mr. Alex Watson for assistance with *in vivo* studies, and Dr. Ganesh Ram Visweswaran for assistance with liposome construction and preliminary work with PyCSP deletion constructs.

REFERENCES

[1] "World malaria report 2022," World Health Organization, https://www.who.int/teams/global-malaria-programme/reports/world-malaria-report-2022 (accessed Jun. 5, 2023).

[2] "CDC - Malaria - Malaria Worldwide - Impact of Malaria," Centers for Disease Control and Prevention, 16-Dec-2021. [Online]. Available: https://www.cdc.gov/malaria/malaria_worldwide/impact.html. [Accessed: 1-Jun-2022].

[3] "Life cycle of the malaria parasite," PATH's Malaria Vaccine Initiative, 20-Feb-2018. [Online]. Available: https://www.malariavaccine.org/malaria-and-vaccines/vaccine-development/life-cycle-malaria-parasite. [Accessed: 10-May-2021].

[4] "WHO recommends groundbreaking malaria vaccine for children at risk," World Health Organization, 06-Oct-2021. [Online]. Available: https://www.who.int/news/item/06-10-2021-who-recommends-groundbreaking-malaria-vaccine-for-children-at-risk. [Accessed: 12-Oct-2021].

[5] M. B. Laurens, "RTS,S/AS01 vaccine (Mosquirix™): An overview," Human Vaccines & *Immunotherapeutics*, vol. 16, no. 3, pp. 480–489, 2019.

[6] S. A. Ogun, L. Dumon-Seignovert, J.-B. Marchand, A. A. Holder, and F. Hill, "The Oligomerization Domain of C4-Binding Protein (C4bp) Acts as an Adjuvant, and the Fusion Protein Comprised of the 19-Kilodalton Merozoite Surface Protein 1 Fused with the Murine C4bp Domain Protects Mice against Malaria," *Infection and Immunity*, vol. 76, no. 8, pp. 3817–3823, 2008.

[7] E. K. Forbes, S. C. de Cassan, D. Llewellyn, S. Biswas, A. L. Goodman, M. G. Cottingham, C. A. Long, R. J. Pleass, A. V. Hill, F. Hill, and S. J. Draper, "T Cell Responses Induced by Adenoviral Vectored Vaccines Can Be Adjuvanted by Fusion of Antigen to the Oligomerization Domain of C4b-Binding Protein," *PLoS ONE*, vol. 7, no. 9, 2012.

[8] A. A. Kaczor and J. Selent, "Oligomerization of G Protein-Coupled Receptors: Biochemical and Biophysical Methods," *Current Medicinal Chemistry*, vol. 18, no. 30, pp. 4606–4634, 2011.

[9] X. Zottig, M. Côté-Cyr, D. Arpin, D. Archambault, and S. Bourgault, "Protein Supramolecular Structures: From Self-Assembly to Nanovaccine Design," *Nanomaterials*, vol. 10, no. 5, p. 1008, 2020.

[10] T. U. Bruun, A.-M. C. Andersson, S. J. Draper, and M. Howarth, "Engineering a Rugged Nanoscaffold To Enhance Plug-and-Display Vaccination," *ACS Nano*, vol. 12, no. 9, pp. 8855–8866, 2018.

[11] C. Mulamba, C. Williams, K. Kreppel, J. B. Ouedraogo, and A. I. Olotu, "Evaluation of the PFS25-IMX313/matrix-M malaria transmission-blocking candidate vaccine in endemic settings," Malaria Journal, vol. 21, no. 1, Jun. 2022. doi:10.1186/s12936-022-04173-y

[12] K. Sliepen, B. W. Han, I. Bontjer, P. Mooij, F. Garces, A.-J. Behrens, K. Rantalainen, S. Kumar, A. Sarkar, P. J. Brouwer, Y. Hua, M. Tolazzi, E. Schermer, J. L. Torres, G.

Ozorowski, P. van der Woude, A. T. de la Peña, M. J. van Breemen, J. M. Camacho-Sánchez, J. A. Burger, M. Medina-Ramírez, N. González, J. Alcami, C. LaBranche, G. Scarlatti, M. J. van Gils, M. Crispin, D. C. Montefiori, A. B. Ward, G. Koopman, J. P. Moore, R. J. Shattock, W. M. Bogers, I. A. Wilson, and R. W. Sanders, "Structure and immunogenicity of a stabilized HIV-1 envelope trimer based on a group-M consensus sequence," *Nature Communications*, vol. 10, no. 1, 2019.

[13] R. Ladenstein and E. Morgunova, "Second career of a biosynthetic enzyme: Lumazine synthase as a virus-like nanoparticle in vaccine development," *Biotechnology Reports,* vol. 27, 2020.

[14] Y. Kato, R. K. Abbott, B. L. Freeman, S. Haupt, B. Groschel, M. Silva, S. Menis, D. J. Irvine, W. R. Schief, and S. Crotty, "Multifaceted effects of antigen valency on B cell response composition and differentiation in vivo," *Immunity*, vol. 53, no. 3, Aug. 2020.

[15] R. Rahikainen, P. Rijal, T. K. Tan, H. J. Wu, A. M. C. Andersson, J. R. Barrett, T. A. Bowden, S. J. Draper, A. R. Townsend, and M. Howarth, "Overcoming symmetry mismatch in vaccine nanoassembly through spontaneous amidation," *Angewandte Chemie*, vol. 133, no. 1, pp. 325–334, 2020.

[16] K. O. Saunders, E. Lee, R. Parks, D. R. Martinez, D. Li, H. Chen, R. J. Edwards, S. Gobeil, M. Barr, K. Mansouri, S. M. Alam, L. L. Sutherland, F. Cai, A. M. Sanzone, M. Berry, K. Manne, K. W. Bock, M. Minai, B. M. Nagata, A. B. Kapingidza, M. Azoitei, L. V. Tse, T. D. Scobey, R. L. Spreng, R. W. Rountree, C. T. DeMarco, T. N. Denny, C. W. Woods, E. W. Petzold, J. Tang, T. H. Oguin, G. D. Sempowski, M. Gagne, D. C. Douek, M. A. Tomai, C. B. Fox, R. Seder, K. Wiehe, D. Weissman, N. Pardi, H. Golding, S. Khurana, P. Acharya, H. Andersen, M. G. Lewis, I. N. Moore, D. C. Montefiori, R. S. Baric, and B. F. Haynes, "Neutralizing antibody vaccine for pandemic and pre-emergent Coronaviruses," *Nature*, vol. 594, no. 7864, pp. 553–559, 2021.

[17] W. Lu, Z. Zhao, Y.-W. Huang, and B. Wang, "Review: A systematic review of virus-like particles of coronavirus: Assembly, generation, chimerism and their application in basic research and in the clinic," *International Journal of Biological Macromolecules*, vol. 200, pp. 487–497, Mar. 2022.

[18] M. T. Mabrouk, W. C. Huang, L. Martinez‐Sobrido, and J. F. Lovell, "Advanced materials for SARS‐COV‐2 vaccines," *Advanced Materials*, vol. 34, no. 12, p. 2107781, Dec. 2022.

[19] M. Q. Rodrigues, P. M. Alves, and A. Roldão, "Functionalizing ferritin nanoparticles for vaccine development," *Pharmaceutics*, vol. 13, no. 10, p. 1621, Oct. 2021.

[20] Jeong HJ, Abhiraman GC, Story CM, Ingram JR, Dougan SK. Generation of Ca2+-independent sortase A mutants with enhanced activity for protein and cell surface labeling. PLoS One. 12(12):e0189068, Dec. 2017.

[21] C. P. Guimaraes, M. D. Witte, C. S. Theile, G. Bozkurt, L. Kundrat, A. E. Blom, and H. L. Ploegh, "Site-specific C-terminal and internal loop labeling of proteins using sortase-mediated reactions," *Nature Protocols*, vol. 8, no. 9, pp. 1787–1799, Aug. 2013.

[22] Y.-N. Zhang et al., “Nanoparticle size influences antigen retention and presentation in lymph node follicles for humoral immunity,” Nano Letters, vol. 19, no. 10, pp. 7226–7235, Sep. 2019. doi:10.1021/acs.nanolett.9b02834.

[23] K. Vijayan et al., “Antibody interference by a non-neutralizing antibody abrogates humoral protection against plasmodium yoelii liver stage,” Cell Reports, vol. 36, no. 5, p. 109489, Aug. 2021. doi:10.1016/j.celrep.2021.109489.

[24] M. Q. Rodrigues, P. M. Alves, and A. Roldão, “Functionalizing ferritin nanoparticles for vaccine development,” Pharmaceutics, vol. 13, no. 10, p. 1621, Oct. 2021. doi:10.3390/pharmaceutics13101621.

[25] J. Ludwig et al., “Glycosylated nanoparticle-based pfcsp vaccine confers long-lasting antibody responses and sterile protection in mouse malaria model,” npj Vaccines, vol. 8, no. 1, Apr. 2023. doi:10.1038/s41541-023-00653-7.